
Electronic Thesis and Dissertation Repository

7-19-2024 9:30 AM

The Use of NP-110, a RHAMM Peptide Mimetic, Reduces Capsule Fibrosis in a Novel Rodent Model of Radiation-Induced Capsular Contracture

Kathryn Minkhorst, *Western University*

Supervisor: DeLyzer, Tanya, *The University of Western Ontario*

: Turley, Eva, *The University of Western Ontario*

: Wong, Eugene, *The University of Western Ontario*

A thesis submitted in partial fulfillment of the requirements for the Master of Science degree in Surgery

© Kathryn Minkhorst 2024

Follow this and additional works at: <https://ir.lib.uwo.ca/etd>



Part of the [Plastic Surgery Commons](#)

Recommended Citation

Minkhorst, Kathryn, "The Use of NP-110, a RHAMM Peptide Mimetic, Reduces Capsule Fibrosis in a Novel Rodent Model of Radiation-Induced Capsular Contracture" (2024). *Electronic Thesis and Dissertation Repository*. 10267.

<https://ir.lib.uwo.ca/etd/10267>

This Dissertation/Thesis is brought to you for free and open access by Scholarship@Western. It has been accepted for inclusion in Electronic Thesis and Dissertation Repository by an authorized administrator of Scholarship@Western. For more information, please contact wlsadmin@uwo.ca.

Abstract

Capsular contracture is a common complication of breast implant reconstructive surgery, which can be particularly devastating in the setting of post-mastectomy radiation. The objective of this thesis was to evaluate the effect of RHAMM function-blocking peptide mimetic NP-110 on a novel rodent model for radiation-induced capsular contracture. The model consisted of female rats who underwent surgery to place a 2cc silicone implant under the right fourth mammary fat pad. The implant, mammary fat pad and overlying skin was radiated. This model was then replicated, and 14 rats received local injection of 100ug of NP-110 or scrambled control peptide followed by 26Gy of targeted ionizing radiation. Clinically, NP-110 treated animals showed decreased post-radiation fibrotic change. Masson's trichrome and Picrosirius red stain showed significantly decreased collagen deposition and bundling in the NP-110 group ($p < 0.001$). Our study concludes that NP-110 significantly reduced capsule fibrosis. Therefore, the RHAMM pathway may be implicated in the development of capsular contracture and could be a potential target for development of preventative therapeutic agents.

Keywords

capsular contracture, breast reconstruction, radiation fibrosis, rat model capsular contracture, collagen deposition, receptor for hyaluronan mediated motility, RHAMM, hyaluronan, RHAMM function-blocking peptides

Summary for Lay Audience

Breast reconstruction is an important part of the patients' breast cancer journey, that has been shown to improve their quality of life. Most commonly, a new breast can be created with the use of silicone implants. Whenever an implant is placed scar tissue forms around the implant. However, in some cases the scar becomes too tight or thick causing disfigurement and making the breast feel hard and sometimes painful. This is especially common when patients have to undergo radiation therapy as part of their breast cancer treatment, and it can be a difficult problem to treat, commonly requiring multiple surgeries and overall less optimal results.

For this study, we used rats as a test subject to better understand the process that leads to excessive scar around an implant after radiation. A total of 14 rats had surgery to place a mini custom implant that mimics the ones used in humans under the rats' breast tissue. Four weeks after surgery half the rats were given an injection of an experimental agent, which is known to block a pathway that leads to scarring. The other half were given an injection of an inactive version of the agent. All the animals then received radiation targeted to the breast tissue and implant.

After radiation, we monitored the rats and inspected the implants for four weeks. After four weeks we collected the implant and surrounding scar tissue to do special tests to measure the amount of scar around the implants. The rats that were treated with the active agent had less collagen in their scars under the microscope using special stains compared to the rats treated with the inactive agent.

Overall, this thesis uses a rat model to learn more about how excessive scarring around an implant happens after radiation. We used an active agent that targets a special pathway, and when this pathway is interrupted, we saw decreased scar around the implant. Therefore, this path may be important in causing the excess scar. There is still more to learn, but this research is a step forward in finding new treatments for this difficult problem.

Co-Authorship Statement

For Chapter 3 and 4: All of the laboratory experiments outlined were performed in Dr. Eva Turley's laboratory. The radiation experiments were performed under the supervision of Dr. Eugene Wong at the London Regional Cancer Program. Natalia Lewandowski and Dr. Tanya DeLyzer assisted with the animal surgery. Natalia Lewandowski also assisted with post-operative and post-radiation monitoring, as well as tissue immunohistochemistry. Carl Postenka paraffinized, embedded, and sectioned all of the mammary fat pad specimens used in the analysis, as well as assisted with Masson's trichrome staining. Caroline O'Neil and Hao Yin from the Molecular Pathology Core Facility at Robarts Research Institute assisted with Picrosirius Red staining.

Acknowledgments

It has been a privilege to complete this thesis and be a part of the Master of Surgery program. I am extremely grateful to the support I have received from the Department of Plastic and Reconstructive Surgery, and all the people who have helped me along the way to allow my successful completion of this thesis.

First of all, I would like to thank all my supervisors, Dr. Tanya DeLyzer, Dr. Eva Turley and Dr. Eugene Wong for their unwavering support, expertise and guidance throughout this process. Dr. Tanya DeLyzer has been a mentor since I started medical school and I would not be where I am today without her. Dr. Eva Turley has provided knowledge and opportunities to learn within the world of basic science I would have not otherwise been exposed to, and I am grateful for her expertise in navigating these concepts. Dr. Eugene Wong was integral to the completion of this project for his development and assistance in the radiation protocol, and dedication to come after hours for radiation delivery.

I would also like to acknowledge Natalia Lewandowski, a medical student who was invaluable for her help with the animal experiments and laboratory work. Her help made completion of this project during residency possible.

The members of the Turley Lab, Conny Tolg and Britney Messan, thank you for your support in the lab and expertise in learning new protocols for this project. Thank you to Carl Potenska for tissue processing, sectioning and staining. Thank you to Caroline O'Neil and Hao Yin for picrosirius staining and training on the polarized microscope at Robarts.

Thank you to my parents, Taylor and all my friends, for all your encouragement and support.

Table of Contents

Abstract.....	ii
Summary for Lay Audience.....	iv
Co-Authorship Statement.....	v
Acknowledgments.....	vi
Table of Contents.....	vii
List of Tables.....	x
List of Figures.....	xi
List of Appendices.....	xiv
Chapter 1.....	1
1 Introduction.....	1
1.1 Definition and Pathogenesis of Capsular Contracture.....	1
1.2 Post Mastectomy Radiation Therapy.....	2
1.3 Radiation Induced Fibrosis.....	3
1.4 Current Management of Capsular Contracture.....	5
1.5 Therapeutic Targets of Interest.....	6
1.5.1 Anti-microbials.....	6
1.5.2 Anti-inflammatories.....	7
1.5.3 Adipose Derived Stem Cells.....	7
1.5.4 Acellular Dermal Matrix.....	8
1.6 Hyaluronan.....	9
1.7 Receptor For Hyaluronan Medicated Motility (RHAMM).....	10
1.8 RHAMM Function Blocking Peptide Mimetics.....	11
1.9 Animal Models.....	12
Chapter 2.....	14

2	Thesis Objectives and Aims.....	14
2.1	Objective 1	14
2.2	Objective 2	14
2.3	Hypothesis.....	15
	Chapter 3.....	16
3	Methods.....	16
3.1	Animal Experiments Overview.....	16
3.1.1	Previous Model Development.....	16
3.1.2	Current Experimental Overview	17
3.2	Surgery Protocol	19
3.2.1	Post-Operative Monitoring	21
3.3	Peptide Preparation and Delivery Protocol.....	22
3.3.1	Peptide Preparation	22
3.3.2	Blinding.....	22
3.3.3	Peptide Injection	23
3.4	Radiation Protocol	24
3.4.1	Post-Radiation Monitoring.....	27
3.5	Tissue Collection	28
3.5.1	Tissue Harvest.....	28
3.5.2	Tissue Processing.....	28
3.6	Tissue Histology	29
3.6.1	Hematoxylin and Eosin.....	29
3.6.2	Masson’s Trichrome	29
3.6.3	Picrosirius Red	30
3.7	Immunohistochemistry	31
3.8	Biochemical Assays	32

Chapter 4.....	34
4 Results	34
4.1 Qualitative Outcomes.....	34
4.2 Masson’s Trichrome	39
4.3 Picrosirius Red.....	42
4.4 Hydroxyproline Assay	45
4.5 Transforming Growth Factor Beta 1 (TGFB1).....	46
4.6 Alpha Smooth Muscle Actin (aSMA).....	50
Chapter 5.....	53
5 Discussion and Conclusion	53
5.1 Objective 1 Discussion	53
5.1.1 Conclusions and Limitations of Objective 1.....	55
5.2 Objective 2 Discussion	57
5.2.1 Conclusions and Limitations of Objective 2.....	61
5.3 Significance and Future Directions.....	62
5.4 Conclusion	63
References.....	65
Curriculum Vitae	73

List of Tables

Table 1: Baker grading score for implant capsular contracture ⁵⁸	22
Table 2. Kumar Score for radiation skin damage ⁵⁹	28
Table 3. Baker grade for all animals in the study pre-radiation, post-radiation week 1, and post-radiation week 4 at the endpoint.	36
Table 4. Kumar score for all animals in the study pre-radiation, post radiation week 1, and post radiation week 4 at the endpoint.	37

List of Figures

Figure 1. Overview of timeline for animal experiments. All animals undergo surgery at day 0, recover for 4 weeks and then are injected with either active peptide NP-110 or scrambled control peptide to the 4th mammary fat pad prior to radiation with 26Gy.	18
Figure 2. Incisions made under the right and left 4th fat pads (A) with demonstration of the sub glandular pocket that was developed (B) and insertion of the implant into the implant pocket after irrigation with betadine solution (C).....	20
Figure 3. “Mini” cohesive silicone gel implants supplied by Mentor/J&J. Base diameter is 2cm, and projection of the implants is 1cm.	21
Figure 4. Injection of peptide solution into the right 4th mammary fat pad of 100uL, for a 100ug dose, directly under the right 4th nipple taking care to not violate the implant capsule.	24
Figure 5. Positioning of a rodent on the 3D printed “Rat-form” showing the targeting of the Orthovoltage unit 3cm cone centered at the implant and fat-pad which lies below the rest of the rats body highlighted by the yellow circle (B).....	26
Figure 6. Radiation film post-radiation showing the radiated field. The top portion shows no penetrance at the shielded area from the lead. The red dashed line highlights the decreased penetrance on the film from the area of the implant and fat pad that was radiated compared to the rest of the field that was empty under the “Rat-form”.	27
Figure 7. Implant site pre-radiation in animal 7 (NP-110) and 4 (control peptide) at A; one week post-radiation, B; two weeks post radiation, C; three weeks post radiation and D; four weeks post radiation (endpoint).	38
Figure 8. Average Kumar scores for animals in the NP-110 and control peptide groups at the end of the study period (4 weeks post-radiation), $p=0.462$ using Mann-Whitney U test.	39

Figure 9. Representative images of paraffin embedded sections of entire capsule and fat pad specimen post sectioning from animal 1 from the NP-110 group (left) and animal 6 from the control peptide group (right). Stained with H&E (top) and Masson’s trichrome (bottom)... 40

Figure 10. Representative images of implant capsule stained with Masson’s Trichrome at 10X magnification. Capsules from the NP-110 group are thinner with less stain (left) compared to the control peptide groups (right)..... 41

Figure 11. Mean grey value of capsule samples, selecting for blue Masson’s trichrome staining for collagen using ImageJ software. Higher mean grey value indicates increased darkness of stain uptake from the sample and therefore increased collagen. There was significantly increased collagen stain in the control peptide group compared to the NP-110 group (p=0.004). 42

Figure 12. Representative images of implant capsule stained with Picrosirius red at 40X magnification. Capsules from the NP-110 group are thinner with less stain (left) compared to the control peptide groups (right). 44

Figure 13. Percent of red pixels per area of capsule samples, selecting for area of the capsules using ImageJ software. Higher percent red pixels indicates increased Picrosirius red stain from the sample and therefore increased collagen deposition and bundling. There was significantly increased red staining in the control peptide group compared to the NP-110 group (p<0.001) when calculated with an independent two-tailed T-test. 45

Figure 14. Ratio of the amount of total protein (ug/well) to hydroxyproline (ug/well) in the NP-110 and control peptide groups capsule + fat pad tissue. There was no significant difference between the NP-110 and control peptide groups (p=0.652). 46

Figure 15. Representative images of TGFB1 immunofluorescence staining of the capsule tissue (A&C) and mammary fat pad (B&D) from an animal treated with NP-110 (A&B) and control peptide (C&D) at 40X magnification. TGFB1 is seen in green with DAPI to stain the nuclei blue. 48

Figure 16. Mean grey value after selecting for green pixels in ImageJ from TGFB1 immunofluorescence of capsule tissue, p=0.592 using Mann Whitney U test. 49

Figure 17. Mean grey value after selecting for green pixels in ImageJ from TGFB1 immunofluorescence stained slides of mammary fat pad tissue, p=0.286 using Mann Whitney U test. 50

Figure 18. Representative images of aSMA immunofluorescence staining of the capsule tissue from NP-110 (left) and control peptide (right) treated animals at 40X magnification. aSMA is seen in green with DAPI to stain the nuclei blue..... 51

Figure 19. Mean grey value after selecting for green pixels in ImageJ from aSMA immunofluorescence of capsule tissue, p=0.103 using Mann Whitney U test. 52

List of Appendices

Appendix 1	Error! Bookmark not defined.
Appendix 2	72

Chapter 1

1 Introduction

Capsular contracture is a common but unpredictable complication of breast implant surgery, which can be particularly devastating in the setting of post-mastectomy and post-lumpectomy breast reconstruction¹. Patients undergoing breast reconstruction and adjuvant radiotherapy are at the highest risk for this complication, with some studies reporting up to 49.4% of patients experiencing significant contracture². Currently, no non-surgical treatment or preventative measures exist to reduce the risk of breast capsular contracture³.

1.1 Definition and Pathogenesis of Capsular Contracture

Breast capsular contracture is currently clinically evaluated with the Baker grading system (Table 1). The scale ranges from grade I (normal capsule), to grade IV (severe painful contracture)⁴. Patients with a grade IV contracture experience firm, painful, disfigured breasts which can lead to psychological distress, further surgery, and the risk of reconstructive failure with implant loss⁴. Revision surgery is especially challenging in patients who received radiation due to the injury and fibrosis it causes to tissue⁵. The consequent risk of reconstructive failure is high, which can be devastating to women attempting to close the loop on their breast cancer journey⁵.

A capsule, which initially forms around implants, is a normal foreign body response of the host tissue that is desirable since it holds the implant in place⁶. However, an excessive fibrotic reaction to this foreign body leads to the development of a thick, dense, collagen-rich capsule that forms the contracture causing significant pain as well as breast deformity³. In general terms, capsular contracture is considered to be initiated by inflammation that becomes chronic, and progresses to excessive fibrosis³. Previous studies have demonstrated that contracted capsules have higher levels of myofibroblasts, that are distributed along the surface contacting the implant, compared to control capsules⁷. Beyond this, the patho-etiology and the molecular mechanisms involved in the

responses to the implant that lead to excessive fibrosis are not well-understood. This knowledge gap and the current limitations of experimental models for radiation-induced capsular contracture in breast tissue has been a barrier to development of effective therapies that either prevent or reduce capsular contracture.

1.2 Post Mastectomy Radiation Therapy

Clinically, numerous studies have demonstrated the deleterious effect of post-mastectomy radiation therapy (PMRT) on implant-based breast reconstruction^{2,5}. Systematic reviews and meta-analyses reported that average incidence of capsular contracture in patients who receive adjuvant radiation therapy to their final implant reconstruction ranged from 43%-49.4%². Patient and surgeon reported cosmetic outcomes were also lower in the radiated compared to non-radiated patient group². If adjuvant radiation is predicted to be required pre-operatively, delayed reconstruction with tissue-expander placement at the time of mastectomy has generally been preferred in an attempt to avoid radiation to the final implant⁸. *In-vitro* studies have suggested that radiation to the implant itself may cause biomaterial alterations, which have been hypothesized to play a role in the development of capsular contracture, although this has not been proven *in vivo*⁹.

However, utilizing a two-stage reconstructive process with tissue expander placement at time of mastectomy, is also not optimal due to a number of complications. The main one being that a delay in implant placement post-radiation does not significantly reduce the incidence of capsular contracture^{8,10,11}. This is likely due to long-lasting epigenetic changes in the tissue microenvironment that result from radiation¹². *In-vitro* studies have shown that irradiation results in irreversible cell senescence, associated with increased secretion of pro-fibrotic cytokines, fibroblast activation and differentiation into myofibroblasts¹¹. Furthermore, although the rates of capsular contracture may be lower when the final implant is placed after radiation, there are some studies that report a higher rate of reconstruction failure when radiation is delivered to the tissue expander¹³. As a result of the number of complications associated with post-mastectomy radiation, many plastic surgeons prefer to avoid implant-based reconstruction in this patient population.

In order to try and prevent some of these complications, there are some studies that are assessing a hypofractionation technique for radiation, which involves an overall lower dose of radiation in a shorter timeline¹⁴. The FABREC trial has shown that at 6 months post-radiation, patients who received the hypofractionation protocol after immediate implant based reconstruction have decreased radiation side effects, without decreased efficacy of the radiation treatment. Although these results are promising, it is known that the onset of capsular contracture can be delayed beyond 6 months, therefore longer follow-up data is needed to assess if this technique causes decreased incidence of capsular contracture in the longer term for these patients⁵.

1.3 Radiation Induced Fibrosis

The impact of radiation on successful reconstruction is becoming more relevant due to the increasing use of radiation therapy to prevent disease recurrence⁸. Immediate breast reconstruction at the time of mastectomy has also become more prevalent, resulting in an increased probability of patients having their implant placed before receiving their final pathology results, and before knowledge of the potential need for radiotherapy⁸.

The molecular mechanisms by which radiotherapy mediates stress-signaling to initially create a pro-fibrotic microenvironment have been well described in the literature. In the acute inflammatory phase, ionizing radiation leads to the transfer of electrons in cells, and as a result generates reactive oxygen species (ROS)¹⁵. These ROS damage cells in multiple ways, including DNA damage and mutation, as well as modifying key proteins and lipids in the cell¹⁵. There is also evidence that cells outside of the radiated field suffer damage, through altered oxidative metabolism, gap junctions, and production of paracrine substances that transmit the damage from radiated cells to nearby 'bystander cells'¹⁵. Damage from the ROS created from ionizing radiation induces cell death and release of damage-associated molecular patterns (DAMPs)¹⁶. DAMPs activate pattern recognition receptors expressed by endothelial and innate immune cells to promote inflammation¹⁶. Persistent inflammation results in changes in the cellular microenvironment and extracellular matrix that ultimately lead to tissue fibrosis¹⁵.

Transforming growth factors (TGFB1-3) are arguably the most prominent factors in promoting fibrosis of irradiated tissues¹². TGFB1 is particularly implicated in radiation-induced fibrosis in experimental models and is a widely expressed cytokine that is primarily sequestered in homeostatic tissues as a latent form bound to the extracellular matrix¹⁷. In its active form, TGFB1 initiates signaling that results in fibroblasts differentiating into myofibroblasts and also increased deposition of collagen that contribute to tissue fibrosis^{17,18}. Activation of TGFB1 is dose-dependent, with higher levels of radiation leading to increased TGFB1¹⁸. Gans *et al.* administered a TGFB1 inhibitor in a mouse model of radiation induced fibrosis, and reported that it mitigated the pro-fibrotic radiation effect seen in control animals¹⁹.

As researchers delve deeper into the signaling pathways involved in this pro-fibrotic pathway, more steps and factors have been elucidated. One important target identified is Smad3, and its activation by TGFB1 signalling²⁰. TGFB1 signals through the transmembrane TGFB type I (TBRI) and TGFB type II (TBRII) receptors²¹. When TGFB1 binds TBRII, TBRI is recruited to form a heterotetrametric complex and is phosphorylated by TBRII²¹. TBRI in turn phosphorylates a number of proteins to activate signaling pathways, including the Smad signaling pathway^{20,21}. The SMAD signaling pathway results in transcription of target genes, and SMAD3 in particular has been linked to increased fibronectin and type I collagen secretion²¹. Animal studies using a mouse model of radiation- induced capsular contracture have shown that Smad3 knockout mice have significantly thinner capsules compared to control, consistent with a key role for TGFB1/SMAD3 in capsular fibrosis²⁰.

Radiation has also been shown to upregulate Thy1 (CD90), a key marker of the differentiation of fibroblasts into contractile myofibroblasts, after exposure to pro-fibrotic stimuli²². When activated, fibroblasts and myofibroblasts express higher levels of alpha smooth muscle actin (ACTA2), and deposit increased collagen that is more tightly bundled²². In the presence of an implant, it is hypothesized that the upregulation of TGFB1 and activation of its signaling pathways, leads to an increase in contractile myofibroblasts and therefore the formation of denser collagen capsules characteristic of capsular contracture^{7,20}. These in-vivo and in-vitro studies provide the basis of our

understanding of the pathways involved in the development of radiation-induced capsular contracture, and point to TGFB1, Smad3 and Thy1 as potential targets in modulating the pro-fibrotic response that leads to this complication.

1.4 Current Management of Capsular Contracture

Clinically, capsular contracture is a difficult problem for surgeons and their patients, as there are often limited options for treatment and unpredictable rates of recurrence. Less invasive techniques include implant massage and other modalities such as diapulse or ultrasound therapy²³. However, there is a lack of evidence in the literature supporting the effectiveness of these therapies²³. As they are non-invasive and with relatively low side-effect profiles, these types of therapies may be offered to individuals with relatively mild capsular contracture or who are not interested in operative management. In the 1970s, the technique of using compression for a closed capsulotomy was described in the literature²⁴. This technique, which was described in breast augmentation patients who developed capsular contracture, has associated complications such as implant rupture, distortion of the breast shape, and recurrent capsular contracture²⁴. As a result, there is little use of this technique in current clinical practice, especially in the setting of breast reconstruction where these complications may be devastating and lead to implant loss, and reconstructive failure.

The current gold standard treatment described in the literature is open or operative capsulotomy and implant exchange³. This involves re-operation to remove the implant, releasing incisions in the capsule (capsulotomy), or removing portions or the entirety of the capsule (capsulectomy), and then replacing with a new implant into the breast pocket. Especially in a submuscular plane, which is the most common in breast reconstruction, the removal of the capsule in its entirety is technically challenging^{25,26}. This operation also carries morbidity as dissecting the capsule from the chest wall can lead to chronic pain, bleeding, and potential damage to the underlying structures²⁶. As a result, many surgeons may opt for a partial over a total capsulectomy, or capsulotomy alone, which releases the tethered capsule without the need for complete dissection^{25,27}. Some studies have reported

that there is no difference in the outcomes and recurrence rate for these two techniques, and therefore it may be up to surgeon preference and patient factors to determine the best approach²⁶. Implant exchange is also commonly recommended in the literature to remove any ruptured or defective devices, or any potential biofilm that may be present on the implant that can be potentially contributing to the development of contracture³.

Unfortunately, as re-operation remains the only option for treatment of capsular contracture, patients must endure additional surgical procedures and recovery time, prolonging their breast cancer journey. Additionally, there is no certainty of resolution even with re-operation, as some studies report up to a 54% recurrence rate of capsular contracture¹. The recurrence rate is especially high in patients who have undergone PMRT compared to those who have not had any previous radiation therapy¹. Furthermore, with re-operation, patients are then re-exposed to the risk of additional scarring, damage to surrounding tissues, wound healing complications, infection, and potentially reconstructive failure³.

1.5 Therapeutic Targets of Interest

A number of therapeutic targets and potential pharmaceutical agents have been tested for the prevention and treatment of capsular contracture, as the scientific community searches for solutions to this pervasive complication.

1.5.1 Anti-microbials

One area of interest in the literature has been the role of bacterial biofilms, which may cause chronic inflammation and therefore be associated with the development of capsular contracture. Rieger et al. showed a positive correlation between cultures from the implant surface and degree of capsular contracture (Baker grade)²⁸. This study placed the implant in an ultrasonic bath with ringers lactate to extract the bacteria off the surface of the implant and then cultured the resulting fluid, a technique specifically used to test for the presence of a biofilm on the implant which is not always detected by traditional culture swabs²⁸. In this study, there was a positive correlation between having a higher grade of

contracture (Baker Grade III or IV) and a positive culture, however not all implants that were associated with severe contracture were positive²⁸. The most common bacteria associated with implant biofilms is *Staphylococcus epidermis*, a commensal skin flora, likely the result of contamination at the time of implantation⁶. Therefore, many surgeons employ aseptic techniques when placing implants in an attempt to mitigate this risk, and there is some evidence that irrigation of the implant pocket with antiseptics decreases the occurrence of severe capsular contracture⁶. There is currently no consensus on the administration of post-operative oral antibiotics, and no strong evidence on the impact of development of capsular contracture⁶. Although there is correlation between the development of capsular contracture and the presence of bacteria or biofilm associated with the implant, it is not present in every case and therefore may be only one risk factor of many in the development of this complication^{6,28}.

1.5.2 Anti-inflammatories

Anti-inflammatory agents, such as leukotriene receptor antagonists, the mast cell stabilizer cromolyn sodium, and corticosteroids, have been identified as agents of interest for prophylaxis of capsular contracture. In one animal study, prophylactic administration of cromolyn sodium, montelukast, and zafirlukast all significantly reduced capsular contracture, with cromolyn sodium being the most effective agent²⁹. In a rabbit model of irradiated implant capsules, montelukast prophylaxis was also seen to decrease capsule thickness, collagen density, and myofibroblast count³⁰. Glucocorticoids broadly reduce pro-inflammatory cytokine and collagen production, and have been shown to decrease TLR activation in a mouse model of capsular contracture⁶. However, large trial clinical data is lacking for any of these treatments, and their systemic administration may produce unwanted side effects that outweigh the potential prophylactic benefit³¹.

1.5.3 Adipose Derived Stem Cells

Recently, adipose-derived stem cells (ADSC) have been recognized in the literature for their antifibrotic properties. Autologous fat grafting is a common procedure done in breast reconstruction where harvested lipoaspirate is injected into the breast. As this procedure has gained popularity there are studies that have shown fat grafting can help to improve

skin quality after radiotherapy³². It is believed that ADSCs are the key component responsible for this clinical effect¹⁵.

As these cells are abundant in healthy donor fat, which is easily harvested through liposuction techniques, there is significant interest in the potential of ADSC to combat fibrosis¹⁵. Experiments using a mouse model of localized scleroderma by Wang et al. showed those treated with ADSC isolates had decreased dermal thickness, as well as decreased expression of TGFB1 and type III collagen³³. These results showed a dose-dependent relationship, with the high dose of ADSCs having the most significant reduction in TGFB1 and collagen type III³³.

Clinical studies have shown that fat grafting at the time of capsule release and implant exchange provide a significant and sustained benefit in resolution of capsular contracture⁵. In some patients who did have persistent capsular contracture, an additional procedure of fat grafting alone lead to resolution of their contracture⁵. Therefore, this suggests that the lipoaspirate, which contains ADSCs, may be beneficial in reducing the radiation-induced fibrosis around the implant. This result is significant, as fat grafting alone is a less invasive procedure compared to capsulotomy and implant exchange and can be done under local anesthesia in some cases, reducing time, cost and risk of anesthetic related complications for the patient⁵. However, more prospective clinical trials are required to further evaluate the benefit of this procedure, as well as clinical data for the use of concentrated ADSC in the treatment of radiation induced capsular contracture.

1.5.4 Acellular Dermal Matrix

The use of acellular dermal matrix (ADM) in breast reconstruction has also increased over recent years, and correlations have been made between decreased rates of capsular contracture and the use of acellular dermal matrix³⁰. In breast reconstruction, acellular dermal matrix is commonly used as a lower pole support for the breast implant not covered by the pectoralis muscle in a submuscular placement, or in some cases to cover and support implant completely for patients requesting a pre-pectoral reconstruction^{34,35}. In vitro models have demonstrated lower levels of proinflammatory markers TNFa and TGFB, as well as CD-68 positive macrophages³⁴. In addition, ADM biopsies showed decreased

fibroblast activity, blood vessel proliferation, collagen disposition and fibrosis when compared to native capsules from the same patients³⁶.

A rabbit study of radiation-induced capsular contracture showed the use of ADM reduced the capsule thickness, collagen deposition and inflammatory markers compared to controls³⁰. Similarly, Kim et al. used a rat model placing silicone implants in a submuscular plane using the latissimus dorsi and covered half the implant with porcine ADM³⁷. The capsule tissue covered by ADM was thinner, and had less staining for α SMA, indicating less fibrosis than the area of capsule covered by muscle³⁷.

The mechanism of ADM preventing capsular contracture is not fully understood. Proposed hypotheses in the literature include: 1) that it creates a physical barrier between the implant and adjacent tissues that contain inflammatory mediators and 2) that it disrupts the normal capsule architecture, creating an island and interfering with the contracture of the capsule as one connected force around the entire implant³. However, these theories have not been properly explored experimentally and further research is needed to understand the potential mechanisms.

1.6 Hyaluronan

A key factor in activation of tissue stress-signaling is fragmentation of the ubiquitous polysaccharide, hyaluronan (HA). HA is a major component of the extracellular matrix, with a variety of functions depending on the molecular weight of the polysaccharide³⁸. Larger molecular weight HA (e.g. >500kDa) has been shown to reduce inflammation, while fragmented lower molecular weight (LMW) HA (e.g. <200kDa) has pro-inflammatory properties, and its accumulation has been associated with fibrosis-based pathologies such as arthritis, diabetes and idiopathic pulmonary fibrosis³⁸⁻⁴⁰.

One mechanism for HA fragmentation is by ROS generated in radiotherapy¹². ROS-generated HA fragments belong to the group of “danger” molecules known as DAMPs, which activate inflammatory pathways⁴¹. HA fragments bind to receptors, in particular CD44, toll-like receptor 4 (TLR4), and the receptor for hyaluronan mediated motility

(RHAMM), which coordinate signaling culminating in the expression TGF β ^{42,43} and other cytokines. The inflammatory and fibrotic stages of tissue remodeling can occur in the presence of a mixture of high, intermediate and low molecular weight fragments⁴⁴.

In a study of patients with capsular contracture, serum levels of hyaluronan was significantly higher than control patients⁴⁵. Furthermore, the level of hyaluronan in the serum (ug/l) was positively correlated with the severity of contracture, with patients with Baker grade III/IV contracture having higher levels of serum hyaluronan compared to patients with grade I/II contracture⁴⁵. Therefore, serum HA is a possible marker for capsular contracture and the development of this complication was postulated to be associated with high HA levels and its fragmentation. This study did not specify the molecular weight of HA, although serum HA is generally low molecular weight⁴⁴. Further studies are necessary to evaluate if serum HA in this patient population is fragmented LMW HA, and if levels are specifically elevated in this population⁴⁵.

Furthermore, although the above mentioned study showed serum HA to be increased with increased severity of capsular contracture, other experiments have shown that HA was decreased in the capsular tissue itself from patients with higher Baker grade contractures^{45,46}. However, this study did not evaluate the molecular weight of HA present in the capsule, and therefore more work is needed to evaluate the role of HA in breast implant capsules and their fibrosis⁴⁶.

1.7 Receptor For Hyaluronan Medicated Motility (RHAMM)

RHAMM (gene name *HMMR*) is an intracellular and extracellular matrix protein that has been implicated in a number of functions, but in the context of capsular contracture, has a role in wound repair, tissue remodeling and fibrosis⁴⁷. The expression of this protein is highly regulated in most tissues and is exported to the cell surface under tissue stress⁴⁸. At the plasma membrane RHAMM partners with CD44 and when bound to HA fragments, activates RAS-ERK1,2 signaling amongst other pathways⁴⁸. Interestingly, RHAMM is not widely expressed in cells during a homeotic state but is transiently

elevated following tissue injury⁴⁹. Loss of RHAMM expression results in aberrant tissue repair⁴⁸. Therefore, RHAMM is a target of interest in understanding and potentially managing disease processes that have an underlying inflammatory or fibrotic pathology.

In the wound environment, RHAMM preferentially binds HA fragments, and these interactions promote fibroblast migration and proliferation as well as increase expression of pro-inflammatory cytokines⁴⁷. The normal cellular infiltration seen in wound models is defective in mice null for *RHAMM*⁴⁹. Furthermore, *RHAMM* knockout fibroblasts and keratinocytes are unable to properly differentiate and migrate, implicating this protein as a key regulator of wound repair⁵⁰. Histological analysis of capsule samples from patients with implants have shown that fibroblasts and myofibroblasts are abundant within the capsule, and a possible over-expression of these cells is thought to be associated with the development of capsular contracture^{51,52}.

However, more work is needed to better elucidate the role of the RHAMM signaling pathway and HA in the development of capsular contracture.

1.8 RHAMM Function Blocking Peptide Mimetics

The role of RHAMM, in its association with low molecular weight HA (LMW-HA) fragments as a regulator of inflammation and fibrosis, has made it an appealing target for a variety of fibrotic diseases such as scleroderma, idiopathic lung fibrosis and arthritis^{39,40,53}. A number of peptide mimetics have been designed and experimentally shown to modulate inflammation, wound repair and fibrosis⁴¹. In cell culture, a peptide mimic, P-15, that was isolated in an unbiased screen for binding to HA fragments, inhibits fibroblast motility in a dose dependent manner. P15 does not have an effect on *RHAMM*-null cells⁴⁷ suggesting it may disrupt RHAMM pro-fibrosis signaling. Consistent with this, in a rat model of excisional skin wounds, P-15 disrupted the pro-inflammatory response that RHAMM-fragmented HA interactions mediate⁴⁷. The expression of TGFB1 and collagen 1 by dermal fibroblasts were significantly reduced in the P-1-treated animals compared to controls⁴⁷.

In a mouse model of scleroderma, the peptide NP-110, which mimics sequence in the HA binding region of RHAMM, reduces dermal thickness, collagen density and hydroxyproline content⁵³. NP-110 appears to act by binding directly to RHAMM to prevent its association with LMW-HA, which ultimately prevents activation of TGF β 1 and the down-stream signaling of this cytokine that leads to fibrosis⁵³. This effect is lost in the absence of RHAMM, as documented by experiments on *RHAMM*-null dermal fibroblasts *in vitro*⁵³. A similar finding was observed in a rat model where the mammary fat pad of the rodents was radiated and at one day post-radiation, received an injection of NP-110 or a scrambled control peptide⁵⁴. The animals that received NP-110 had reduced TGF β expression compared to the control⁵⁴. Histological analysis of the fat pad also showed decreased fibrosis and collagen deposition in NP-110 treated vs control animals, as well as an increase in adiponectin, a marker of adipogenesis whose expression is linked to anti-inflammatory environment⁵⁴.

1.9 Animal Models

Several animal models have been reported to evaluate the pathogenesis and potential treatment modalities for capsular contracture. Models include the use of mice, rats, and rabbits^{30,55,56}. Previously, silicone blocks, or lab-made implant replicas were used in lieu of industry standard silicone implants⁵⁷. In more recent years, mini cohesive silicone gel implants have been used to more precisely replicate the material used in human breast surgery^{29,30}. However, the majority of these studies place the implant on the dorsal surface of the animals back and therefore do not replicate the local tissue micro-environment of mammary tissue³⁰.

In radiation models, there is a variety of doses of ionizing radiation used in the literature. Doses range from 5Gy to 35Gy, however the species used in the model can impact the result. In rats, Kim et al., tested multiple doses of radiation of 10-, 20- and 35-Gy and found 35Gy delivered in 5 fractions of 7Gy induced significant histologically detected fibrotic changes in the capsule around a mini silicone gel implant placed dorsally in a submuscular pocket using the latissimus dorsi³⁷. Their group also tested a higher dose of

45Gy and found this to be fatal to the animals . A limitation of this study includes the dorsal placement of this implant, which may affect the microenvironment of the capsule and development of radiation induced capsule fibrosis.

Truong et al. developed a model for radiation-induced rodent mammary fat pad fibrosis⁵⁴. In the development of this model, 26Gy of ionizing radiation could be delivered in a single fraction, without systemic illness or animal fatality⁵⁴. This was a sufficient dose to elicit local skin changes, and other indicators of fibrosis including increased collagen deposition and bundling in the fat pad, as well as TGFB1 expression on the fat pad⁵⁴.

Based on the previous work done by Truong *et al*, DeLyzer *et al* developed a radiation-induced rat model of capsular contracture with implants placed in a pocket created under the mammary fat pads^{54,58}. This novel model uses custom mini silicone implants replicating those used in human breast reconstruction. Implants were placed beneath the 4th mammary fat pad and a one-time 26Gy dose targeted radiation therapy was delivered to the fat pad and implant using a 3D-printed “ratform” 4 weeks post-surgery⁵⁸. Capsular contracture was induced in this model, and was measurable by clinical exam, tissue histology and fibrosis biomarker assays⁵⁸.

Chapter 2

2 Thesis Objectives and Aims

2.1 Objective 1

Replicate the previously developed rodent model for radiation-induced implant capsular contracture using the standardized procedures as outlined in the thesis work of T.

DeLyzer et al. with the addition of injection of NP-110 or a scrambled control peptide to the mammary fat pad.

Aim 1: Replicate the standardized surgical procedure to place a silicone prosthesis under the right 4th mammary fat pad.

Aim 2: Develop a standardized blinded procedure to deliver a one-time dose of 100ug of active NP-110 peptide or inactive control scrambled peptide to the right 4th mammary fat pad based on previous protocols from Truong *et al*

Aim 3: Replicate the standard radiation protocol developed by DeLyzer *et al* to deliver a targeted one-time dose of 26Gy radiation using the custom ‘ratform’.

2.2 Objective 2

Evaluate the effect of local NP-110 injection into the mammary fat pad tissue on implant radiation-induced capsule fibrosis compared to an inactive control peptide, radiation alone, and non-radiated capsules.

Aim 1: Evaluate radiation changes clinically using Baker grade and Kumar score.

Aim 2: Use paraffin embedded sections of the implant capsule tissue with adjacent fat pad and stain for Masson’s trichrome and Picrosirius red to evaluate collagen deposition and bundling within the capsule. Compare the collagen deposition and bundling between the NP-110 and control peptide groups.

Aim 3: Use hydroxyproline and total protein assays to evaluate for the collagen content in the implant capsule and fat pad and compare between the NP-110 and control peptide groups.

Aim 4: Compare the results from the histological staining as well as assay data from the NP-110 and control peptide groups to the previously published data from DeLyzar *et al* of radiated and non-radiated capsules with no peptide treatment.

2.3 Hypothesis

It is hypothesized that the peptide mimetic NP-110 will decrease radiation-induced capsule fibrosis in this novel rodent model of radiation-induced implant capsular contracture implicating the RHAMM pathway will as a therapeutic target for capsular contracture.

Chapter 3

3 Methods

All experiments were approved and compliant with the standard operating protocols (SOP) of the Animal Use Subcommittee (Protocol # 2022-126) at Western University in London, Ontario, Canada.

All animal work was conducted at London Health Sciences Centre, London Regional Cancer Program (LRCP), and Victoria Research Laboratory (VRL).

3.1 Animal Experiments Overview

3.1.1 Previous Model Development

Based on the previous work done in the Turley lab by Truong *et al*, DeLyzer *et al* previously developed a novel rat model of radiation-induced capsular contracture^{54,58}. In this model, custom 2cc silicone implants (J&J, Mentor) were placed in a sub-mammary fat pad pocket (right 4th mammary fat pad). This model uses custom mini silicone implants replicating those used in human breast reconstruction⁵⁸. Implants are placed under the 4th mammary fat pad and a one-time 26Gy dose targeted radiation therapy is then delivered to the fat pad and implant using a 3D-printed “ratform” 4 weeks post-surgery⁵⁸. Capsular contracture is induced in mammary fat pad in this model, and is measurable by clinical exam, tissue histology and fibrosis biomarker assays⁵⁸. This model is the basis for the experimental design utilized in the current project. The model showed significantly increased fibrosis in the radiated capsules at a dose of 26Gy⁵⁸.

Sample Size Calculation

A previous power-analysis and sample size calculation was performed to determine the number of animals needed per group seen below:

$$\text{Sample size} = 2 (Z_{\alpha/2} + Z_{\beta})^2 \times P(1 - P)/(p1 - p2)^2$$

A power of 0.8 and significance level of $p < 0.05$ was used. The endpoint used was the development of clinically detectable capsular contracture. The prevalence in the case (radiated) group (p_1) was assumed to be 100% or 1.0, and the prevalence in the control (non-radiated) group (p_2) 20% or 0.2 based on the rate in the literature of development of capsular contracture without radiation.

$$Z_{\alpha/2} = Z_{0.05/2} = Z_{0.025} = 1.96 \text{ (From Z table) at type 1 error of 5\% } Z_{\beta} = Z_{0.20} = 0.842 \text{ (From Z table) at 80\% power}$$

$$P = \text{Pooled prevalence} = (\text{prevalence in case group } [p_1] + \text{prevalence in the control group } [p_2])/2 = (1 + 0.2)/2 = 0.6$$

$$\text{Sample size} = 2 (Z_{\alpha/2} + Z_{\beta})^2 \times P (1 - P)/(p_1 - p_2)^2 = 2(1.96 + 0.842)^2 \times 0.6 (1 - 0.6)/(1 - 0.2)^2 = 5.88.$$

Based on these calculations, a sample size of 6 animals per group was required. To account for possible attrition of 10% each group sample size was set at 7 animals. Using this sample size for the previous study, DeLyzer *et al* had statistically significant contracture measured in the implant capsules from radiated animals compared to the control, non-radiated group^{58,59}.

3.1.2 Current Experimental Overview

An overview of the timeline for the experiments is shown below in Figure 1. Experiments were conducted using Sprague Dawley retired female breeder rats (Charles River). All the animals were similar in size and weight, although the exact age could not be provided, Charles River retired breeder rats are typically 6-12 months of age. Rats were caged in pairs, in a temperature-controlled room, with a 12-hour light/dark cycle, and were provided water and a standard rat diet in addition to sunflower seeds and enrichment items. Fourteen rats underwent implant surgery (described below), then received targeted radiation to the implant 4 weeks post-operatively. At the time of radiation, while under anesthetic, the rodents were given a 100ug dose of experimentally active peptide, or a scrambled control peptide (active peptide, control peptide). The peptide was delivered as

an injection targeted under the nipple subcutaneously to the right fourth mammary fat pad above the implant. The researchers in the study were blinded to which animals received the active or control purposes for both the duration of the animal experimental period and all following analysis. The endpoint of the study was pre-determined to be four weeks post-radiation based on the previous model development, as this allowed for clinically and histologically measurable development of capsule fibrosis. All the animals were monitored weekly for health and weight and pre-determined criteria for removal of the animal from the study was set in consultation with animal veterinary services at Western University.

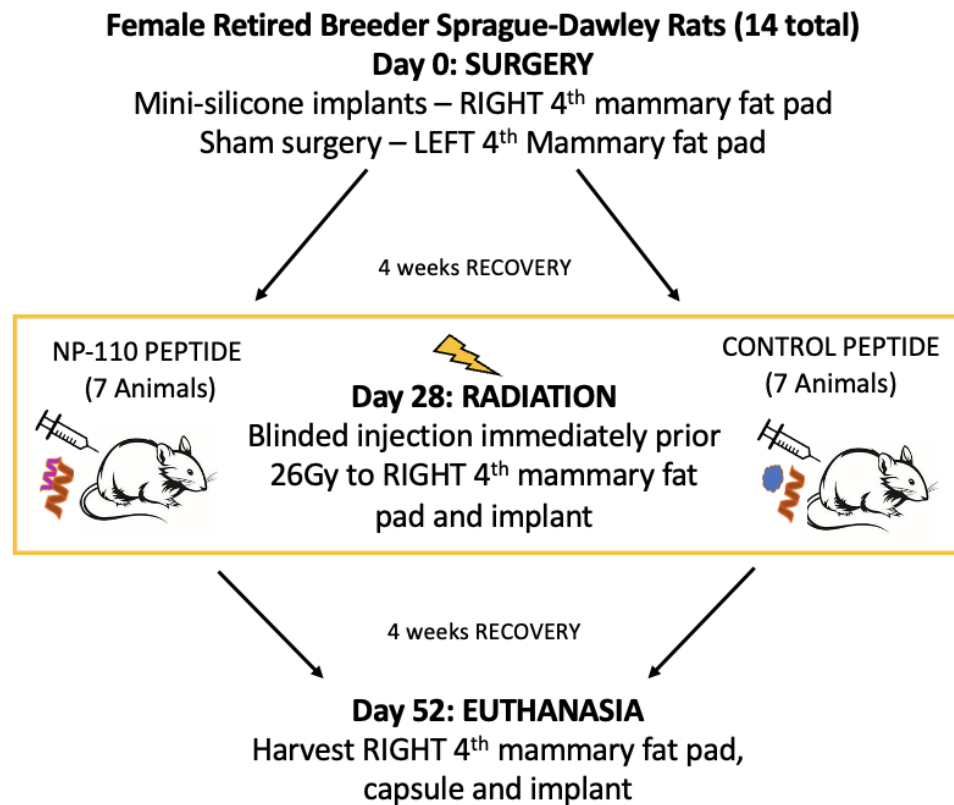


Figure 1. Overview of timeline for animal experiments. All animals undergo surgery at day 0, recover for 4 weeks and then are injected with either active peptide NP-110 or scrambled control peptide to the 4th mammary fat pad prior to radiation with 26Gy.

3.2 Surgery Protocol

Surgery was conducted at the LRCP VRL animal facilities. Animals were induced isoflurane gas anesthesia in an induction chamber. Once sedated the animals were transferred to a warmed operating table and maintained via a nose cone with isoflurane gas for the surgery (Figure 2). Animals were administered a single dose of Meloxicam (1-2mg/kg) subcutaneously while under anesthesia prior to operative positioning. Rats were positioned supine on a warming pad and limbs secured in position with tape. Lubricant was used to protect the eyes. Temperature was then measured. Hair over the 4th set of mammary fat pads was then clipped in a 2cm diameter centered around the nipple. Skin was prepped with antiseptic scrub (chlorhexidine) followed by alcohol wipe and then final application of antiseptic solution (betadine). This procedure was repeated twice prior to incision. On the right and left side, an incision was made through the skin and subcutaneous tissue below the 4th mammary fat pad, a pocket was then dissected below the fat pad with scissors (Figure 2). On the right side, a 2cc custom “mini” cohesive silicone gel implant (Mentor, Johnson&Johnson) was placed in the pocket after being irrigated with betadine. Dimensions of the implant are 2cm diameter and 1cm projection (height) (Figure 3). On the left side, no implant was placed (sham surgery). The incisions on both sides were then closed with an absorbable 5-0 vicryl suture and secured with skin glue. Animals were then administered oxygen vis nose cone until awoken from anesthesia and then transferred to a clean bed for recovery. Once appropriately recovered, animals were transferred back to their regular caging.



Figure 2. Incisions made under the right and left 4th fat pads (A) with demonstration of the sub glandular pocket that was developed (B) and insertion of the implant into the implant pocket after irrigation with betadine solution (C).

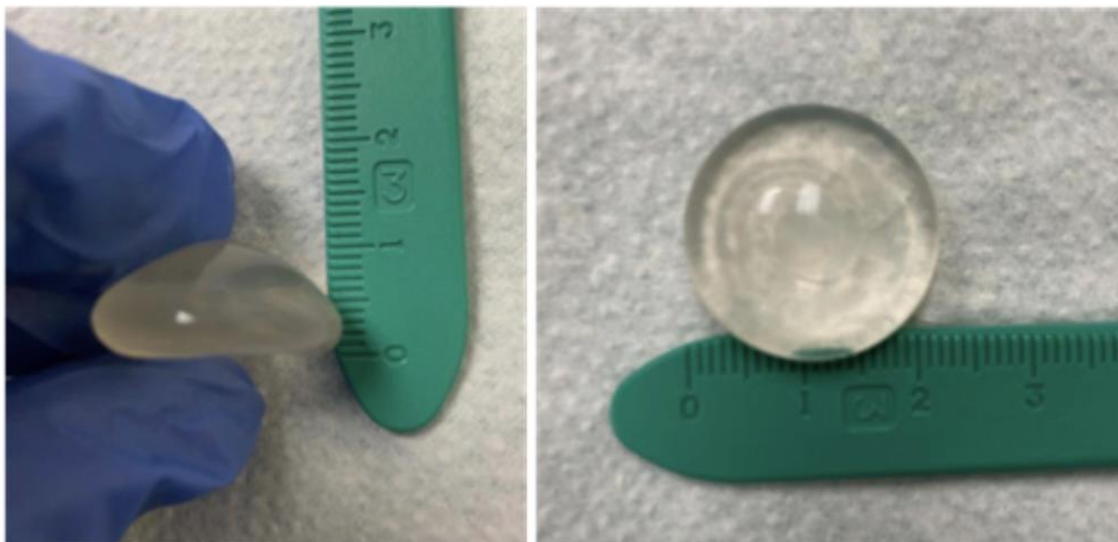


Figure 3. “Mini” cohesive silicone gel implants supplied by Mentor/J&J. Base diameter is 2cm, and projection of the implants is 1cm.

3.2.1 Post-Operative Monitoring

Animals were monitored daily for the first 7 days post-operatively and then weekly thereafter. Weight was recorded along with recording body condition score and a standardized scoring template for behavior, appearance, activity, and dehydration and pain. The surgical site was also examined and assessed site for complications. The implant was examined weekly for evidence of capsular contracture and given a Baker grading score using the criteria described in Table 1 below. In our study we scored Baker grade from 1-3 as a grade 4 contracture requires pain to be present, and could therefore not be accurately assessed in our model. All assessments were performed by K. Minkhorst or N. Lewandowski.

Table 1: Baker grading score for implant capsular contracture⁴.

Baker Grade	Description
I	Soft, mobile implant
II	Implant is palpable but not visible
III	Implant is easily palpable, and visible
IV	Implant is hard, distorted, and painful

3.3 Peptide Preparation and Delivery Protocol

3.3.1 Peptide Preparation

The NP-110 active peptide and scrambled control peptide were prepared in the Luyt lab. The active peptide sequence is Ac-KLKDENSQKSEVSK-NH₂ and has been previously verified to prevent RHAMM signaling. The scrambled control peptide, identified as NP-0111 by the Luyt lab contains the same amino acids as the active NP-110 in alternate sequences with an identical molecular weight which were verified using mass spectrometry. The exact mass was provided labelled on the vial. The peptides were stored in the -80 degree Celsius freezer during the study period. The peptide was prepared for injection by dissolving of 1000ug peptide in 1000uL Hank's Solution using sterile technique to create a final dilution of 1ug/uL. The prepared peptide was stored in the -80 degree Celsius freezer until use.

3.3.2 Blinding

Prior to peptide preparation, the vials were labelled A and B by an individual not involved in any experiments or analysis. All individuals involved in any experiments, and analysis were kept blind until the completion of all experiments and data analysis. Once at the study endpoint, the investigators were unblinded to which group received the active peptide NP-110 and which group received the scrambled control peptide.

3.3.3 Peptide Injection

Animals were first induced using isoflurane as per our SOP. Once a deep anesthesia was achieved, the animals were transferred to the radiation platform, and placed supine with a nose cone for maintenance anesthesia. The skin over the right mammary fat pad was prepped with an alcohol swab and 100uL of peptide solution was injected subcutaneously in the mammary fat pad directly under the right 4th nipple. Care was taken to deliver the peptide directly into the fat pad without violating the implant pocket. This was done by using tweezers to lift the right 4th nipple and tent up the skin. The 30g needle was then introduced under the nipple into the fat pad until the bevel was subcutaneous (Figure 4). A total of 100uL of peptide solution was injected for a dose of 100ug of active NP-110 or control scrambled peptide. Odd numbered animals received the peptide labelled 'A' (group A) and even numbered animals received the peptide labelled 'B' (group B).



Figure 4. Injection of peptide solution into the right 4th mammary fat pad of 100uL, for a 100ug dose, directly under the right 4th nipple taking care to not violate the implant capsule.

3.4 Radiation Protocol

Radiation was conducted under the supervision of an experienced medical physicist, Dr. Eugene Wong, in the London Regional Cancer Centre using a clinically active orthovoltage unit. A total of 26 Gy was delivered in one session. 13Gy was delivered from the right side and 13Gy from the left side, targeted to the implant and overlying right 4th mammary fat pad. No radiation was delivered to the left 4th mammary fat pad “sham surgery” side. After peptide injection was complete, the animals were positioned prone on the custom 3D printed ‘Rat-form’ which allowed for only the implant, and overlying fat pad and skin to be in the radiation field (Figure 5). The body of the rodent

was shielded with a lead shield. A 3cm cone was attached to the orthovoltage radiator and was placed directly in contact with the side of the radiation cage. The implant and surrounding tissue were centered in the middle of the cone. A tester film was also placed on the far side of the cage for some of the animals, which turns dark when exposed to radiation, to ensure the beam was penetrating effectively (Figure 6). Each side of the right 4th mammary fat pad and implant received 3360 MU which corresponded to 13 Gy dose. This was done in two sessions one from the left lateral position of the animal, and then the cage was flipped and the second dose was received from the right lateral aspect of the animal, for a total of 26Gy. The penetration of the Orthovoltage unit is approximately 4-6cm, which is well above the span of the 2cm implant and therefore appropriate to penetrate for this study. The total session took approximately 12 minutes per side of radiation time, for 24 minutes total. The animals were monitored for breathing and signs of movement during the entire session using video monitors. Post-radiation, animals temperature was recorded and were recovered in individual cages to ensure safe recovery from anesthesia.



Figure 5. Positioning of a rodent on the 3D printed “Rat-form” showing the targeting of the Orthovoltage unit 3cm cone centered at the implant and fat-pad which lies below the rest of the rats body highlighted by the yellow circle (B).

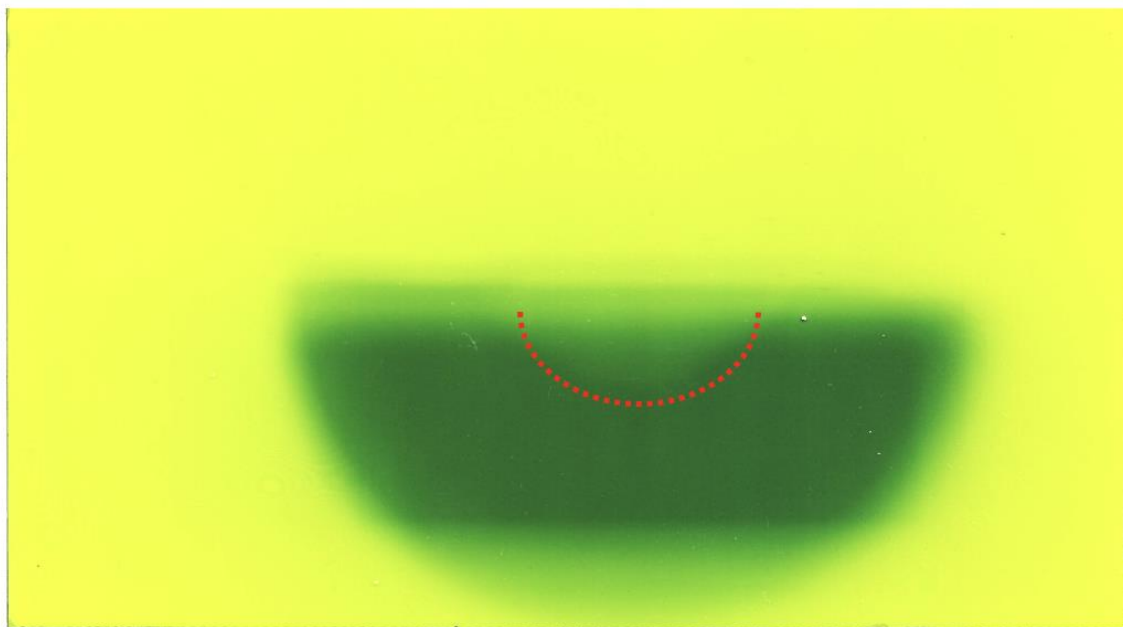


Figure 6. Radiation film post-radiation showing the radiated field. The top portion shows no penetrance at the shielded area from the lead. The red dashed line highlights the decreased penetrance on the film from the area of the implant and fat pad that was radiated compared to the rest of the field that was empty under the “Rat-form”.

3.4.1 Post-Radiation Monitoring

Animals were monitored daily for the first 7 days post-radiation and then bi-weekly thereafter. Weight was recorded along with recording body condition score and a standardized scoring template for behavior, appearance, activity, and dehydration and pain. The surgical site was also examined and assessed site for complications. The implant continued to be examined bi-weekly and scored using the Baker grade scale (Table 1). The animals abdomen was also examined and scored using the Kumar Score for radiation skin changes seen in Table 2. All assessments were performed by K. Minkhorst or N. Lewandowski.

Table 2. Kumar Score for radiation skin damage⁶⁰.

Kumar Score	Skin Changes
1	No effect
1.5	Minimal erythema, mild dry skin
2	Moderate erythema, dry skin
2.5	Marked erythema, dry desquamation
3	Dry desquamation, minimal dry crusting
3.5	Dry desquamation, dry crusting, superficial minimal scabbing
4	Patchy moist desquamation, moderate scabbing
4.5	Confluent moist desquamation, ulcers, large deep scabs
5	Open wound, full thickness skin loss
5.5	Necrosis

3.5 Tissue Collection

3.5.1 Tissue Harvest

At four weeks post-radiation, the animals were euthanized with isoflurane overdose per SOP protocol. A final weight, photo of the area, and Baker score was recorded. The right 4th mammary fat pat, implant and capsule were dissected and removed en bloc to preserve local tissue architecture using a 15 blade. The left 4th mammary fat pad was also harvested at the time of dissection for possible future studies. All tissue was placed in 10% neutral buffered formalin (NBF) immediately after harvest for fixation. Animals were disposed of as per animal care protocol.

3.5.2 Tissue Processing

The en bloc tissue sample containing the implant, capsule and fat pad were fixed in 10% NBF and then processed using serial dehydration by the Lawson department histologist, Carl Potenska. The left sham surgery mammary fat pads were also dissected en bloc using the mammary artery and 4th nipple as landmarks. The fat pad was placed in 10%

NBF for fixation. These samples were then embedded in paraffin wax with the implant in situ. These provisional blocks were sectioned, then the implants were removed and the area remaining was filled with paraffin. The blocks were re-heated and cooled twice to promote integration of the paraffin. Therefore, the structure of the capsule around the implant was preserved. Sections were taken at 10 microns and transferred to slides.

The left sham surgery mammary fat pads were fixed in 10% NBF and then processed using serial dehydration by the Lawson department histologist, Carl Potenska. These samples were then embedded in paraffin wax for preservation, however for the purposes of this thesis, no sections were taken as the studies are focusing on the implant and capsule side.

3.6 Tissue Histology

All histological stains are performed on sections taken from the implant capsule and right 4th mammary fat pad tissue.

3.6.1 Hematoxylin and Eosin

Tissue sections were stained with Hematoxylin and Eosin (H&E). Sections from all animals in the study were included. Two slides per animal were stained, one superficial and one deeper section. Image acquisition was conducted using an Aperio ImageScope, (Leica Microsystems, Buffalo Grove, IL, USA) and associated software was used to capture images of each slide. One image of the entire slide, and a representative image of the capsule at 10X magnification were taken.

3.6.2 Masson's Trichrome

Tissue sections were stained for collagen using Masson's Trichrome (Cat # HT15-1KT, Sigma-Aldrich, Darmstadt, Germany). Five sections of the implant side (right) at varying depths were stained for each animal in the study. Image acquisition was conducted using an Aperio ImageScope, (Leica Microsystems, Buffalo Grove, IL, USA) and associated software was used to capture images of each slide. Images of the entire slide, as well as

four randomly selected images at 10X magnification were taken of areas that contained capsular tissue and adjacent fat pad. If there was damaged tissue, overlapped tissue, or the area was not properly focused, another area was chosen. Masson's trichrome highlights collagen fibers, with collagen staining blue. Increased blue staining indicates greater collagen content in the tissue sample.

Image analysis was carried out using ImageJ software (U.S. National Institute of Health, Bethesda, Maryland, USA). Images were de-convoluted using the pre-programmed function for Masson's Trichrome and the image selecting for blue pixels was used. The polygon function was used to select for the area containing capsular tissue. The size of the area containing capsular tissue and the mean grey value of this area was measured. The mean grey value for 20 regions of interest (ROIs) for each animal were averaged, with higher grey values corresponding to more stain uptake, and thus higher collagen content.

3.6.3 Picrosirius Red

Tissue sections were stained for collagen using Picrosirius Red Staining Kit (Cat # 2490-250, Polysciences, Warrington, PA) with the help of the Molecular Pathology Lab at Robarts Research Institute. Five sections at varying depths of the implant side (right) per animal were stained. Slides were examined under polarized light and four ROIs at 40X magnification were taken of each slide, focusing on capsular and adjacent mammary fat pad. Abrio 2.2 (Cri, Woburn, MA, USA) software was used for image acquisition. Images were captured by a blinded assessor and saved in Pseudocolor format.

Analysis was carried out using ImageJ software (U.S. National Institute of Health, Bethesda, Maryland, USA). Under polarized light, there is differing birefringence colours that are dependent on collagen fiber thickness and alignment. Increasing fiber thickness is observed through changes in colour from blue to yellow to orange to red. Thus, expression of red, or denser collagen bundling in the tissue is typical of fibrosis. The image was split into channels using the RGB stack function and the red channel was selected. The threshold function in ImageJ was used and the threshold was set to 220-255 to capture red stained tissue. The polygon function was then used to outline the area

containing capsular tissue. The percentage of the area selected containing red pixels as detected by set threshold was measured. The percent area for 20 ROIs per animal were averaged.

3.7 Immunohistochemistry

The TGFB and aSMA immunohistochemistry staining of the capsule tissue was performed following a 3-day protocol. For each antibody, 42 slides were stained (3 for each animal). On day 1, the tissue was first de-paraffinized and rehydrated. A 15-minute xylene wash was used to remove paraffin, followed by a second 15-minute xylene wash to account for any remaining paraffin. Next, a 10-minute wash in 100% ethanol removed the xylene, followed by a 10-minute wash in 95% ethanol, and then a 10-minute wash in 70% ethanol to dehydrate the specimen. The tissue was then placed in distilled water for 5 minutes to rehydrate. Finally, 1x TBS (or 1x PBS) was used to wash the specimen for 5 minutes. Antigen retrieval was performed using 10mM sodium citrate titrated to a pH of 6.0. The solution was prepared using 1.47g of sodium citrate and 400mL distilled water. pH was adjusted to 6.0 using HCL and then the solution was brought to a volume of 500mL using distilled water. Antigen was retrieved by microwaving the tissues on power level 10 for 3 minutes, then on power level 5 for 5 minutes, and then on power level 3 for 8 minutes. The slides were then cooled for 30 minutes and afterwards, washed in 1x TBS for 10 minutes. Afterward, the slides were blocked with 3% BSA diluted in 1x TBS (or 1x PBS) for 1 hour. The BSA was prepared by dissolving 3g of albumin in 100mL of 1x TBS (or 1x PBS). The tissue on each slide was then encircled with wax and 50uL of primary antibody was pipetted onto it. The primary TGF beta 1 antibody used was Abcam Recombinant Anti-TGF beta 1 antibody (Cat # ab215715, Abcam, Bristol, United Kingdom) and the aSMA antibody used was Abcam Recombinant Anti-alpha smooth muscle Actin antibody (Cat # ab124964, Abcam, Bristol, United Kingdom). Both primary antibodies were diluted in 1 x TBS at a concentration of 1:100uL. The slides were then left overnight in tinfoil humidifiers in a 4 degrees Celsius fridge. On day 2, the slides were washed in the 1 x TBS (or PBS) solution for 10 minutes. Next, the tissues were re-surrounded by wax and 50uL of secondary antibody diluted in 1 x TBS at a

concentration of 1:100uL was pipetted onto each. The secondary antibody used was Invitrogen Goat anti-Rabbit IgG (H+L) Highly Cross-Adsorbed Secondary Antibody, Alexa Fluor™ 488 (Cat # A-11034, Thermo-Fisher, Waltham, MA, USA). Slides were then incubated in the tinfoil humidifiers at room temperature for 2 hours, followed by a 10-minute wash in 1 x TBS (or PBS). Finally, 2-3 drops of Invitrogen™ ProLong™ Gold Antifade Mountant (Cat # P36930, Thermo-Fisher, Waltham, MA, USA) with DNA Stain DAPI (Cat # D1306, Thermo-Fisher, Waltham, MA, USA) were added to each slide and coverslips were applied, making sure to eliminate air bubbles. Slides were then stored in the tinfoil humidifiers at room temperature for next-day imaging. The slides were imaged on day 3 of the protocol using the Olympus Fluoview microscope and associated Fluoview computer program (Olympus, Shinjuku City, Japan).

3.8 Biochemical Assays

The second method of quantifying fibrosis in the tissue samples was through tissue hydrolysis assays for hydroxyproline (Cat # ab222941, Abcam, Bristol, United Kingdom) and total protein (Cat #QZBtotprot1, Quickzyme Biosciences, Leiden, Netherlands). The amount of hydroxyproline in a tissue sample was used as a measurement of collagen, and standardized against the amount of total protein in the sample to account for any difference in the amount of tissue in each of the hydrolysates. A higher ratio would indicate higher collagen content and thus, more fibrosis.

Tissue samples were prepared and hydrolyzed using 6N HCl and heated for 16 hours and 95 degrees Celsius. Twenty-five 10uM sections from the right 4th implant capsule and mammary fat pad from each animal in both groups were used. The stock hydrolysate solution was centrifuged at 13 000 rpm for 10 minutes to separate it from the paraffin wax, and the resulting supernatant was pipetted into an Eppendorf tube. The stock hydrolysate was serially diluted using 6N HCl. A test assay was run with the standard to pick a dilution that fit within the standard curve. The dilution that best fit within the curve was 1/16 for both the hydroxyproline and total protein assays. Six technical replicates were run per sample.

Standards were prepared according to manufactures instructions. The standards and experimental sample assays were run in 96-well plates, and absorption was read at 570nm and 560nm for total protein and hydroxyproline respectively using Biotek plate reader Synergy HTX (Biotek Instruments, Winooski, Vt, USA). The standard curve was then used to calculate the concentration of hydroxyproline (ug/uL) and total protein (mg/mL) per well. The average concentrations of the technical replicates were calculated, excluding any outliers. The average for each animal were then used to calculate the overall ratio of hydroxyproline to total protein for each sample.

Chapter 4

4 Results

4.1 Qualitative Outcomes

Fourteen female retired breeder Sprague-Dawley rats were included in the study. All the animals were similar in size, with weight ranging from 285g to 390g with an average weight of 332g. Animal 9 was noted to have a soft tissue mass to the right upper limb. We consulted with the veterinary team as per VRL protocols, and their team deemed it to be acceptable to be monitored without removing the animal from the study. The mass was monitored throughout and remained similar in size and shape, was soft and mobile, and did not impact function or movement of the rodent. It was at a distance from the operative and treatment site. Therefore, this animal was included in the study to the endpoint. There was no loss of animals during our study due to complications from surgery, radiation or other illness.

Surgery was completed as per protocol without any complications. All animals were monitored post-operatively, and there were no infections, wound healing issues, or other late complications.

At the time of radiation, there was a mechanical issue with the anesthetic machine, which failed during radiation of animal 3 (NP-110 group). Due to this failure, animal 3 only received a partial dose of radiation from the left side, and the protocol had to be aborted early. We continued to monitor this animal to the end point but removed the data from analysis due to incomplete radiation treatment. All other animals completed radiation without any complications.

In terms of qualitative assessment, all animals healed well from surgery and all implants were soft and mobile, Baker grade 1, prior to radiation (Table 3). One-week post-radiation, there were some mild radiation changes noted, however all implants remained Baker grade 1 (Table 3). At four weeks post-radiation, radiation changes as assessed by Kumar score, and Baker's grade increased for all animals (Table 3 and 4).

All animals in the control peptide group developed a grade 3 contracture, whereas two animals in the NP-110 group developed only grade 2 contracture following radiation treatment. Grade 2 contractures were qualitatively a more visible implant on the animal's abdomen, which had decreased mobility compared to pre-radiation. Grade 3 contractures were those with a more visible implant, which had significantly decreased mobility compared to pre-radiation. As seen in the representative images in Figure 7, post-radiation week 1 and 2 showed minimal change in both groups. By week 3 and 4 post-radiation, there was more significant hair loss, desquamation and ulceration in some animals. By the endpoint, the animals in the control peptide group had more visible contractures overall compared to the NP-110 group (Figure 7). All radiated animals had some skin changes and hair loss, as evaluated by Kumar score (Table 4) However, on average the Kumar score of the NP-110 group was lower than the control peptide group, although this result was not significant (Figure 8). At the time of tissue harvest, it was also noted that the animals in the control peptide group were more difficult to dissect, as the capsule was more adhered to the surrounding tissue, especially on the muscular layer.

The left contralateral mammary fat pad sham surgery incisions healed well. Some of the animals had some central hair loss, however this was minimal. There was no visible skin redness or ulceration on the left side. Therefore, this indicates mild radiation effects outside of the field targeted for radiation. However, these effects were mild, and the significant changes were all seen within the targeted area of the right 4th mammary fat pad and implant.

Table 3. Baker grade for all animals in the study pre-radiation, post-radiation week 1, and post-radiation week 4 at the endpoint.

Treatment Group	Animal ID	Pre-Radiation	Post-Radiation Day 7	Post-Radiation Week 4
NP-110	1	1	1	2
	5	1	1	3
	7	1	1	3
	9	1	1	2
	11	1	1	3
	13	1	1	3
Control Peptide	2	1	1	3
	4	1	1	3
	6	1	1	3
	8	1	1	3
	10	1	1	3
	12	1	1	3
	14	1	1	3

Table 4. Kumar score for all animals in the study pre-radiation, post radiation week 1, and post radiation week 4 at the endpoint.

Treatment Group	Animal ID	Pre-Radiation	Post-Radiation Day 7	Post-Radiation Week 4
NP-110	1	1	1	2
	5	1	1	3
	7	1	1	3
	9	1	1	2
	11	1	1	3
	13	1	1	3
Control Peptide	2	1	1	3
	4	1	1	3
	6	1	1	3
	8	1	1	3
	10	1	1	3
	12	1	1	3
	14	1	1	3

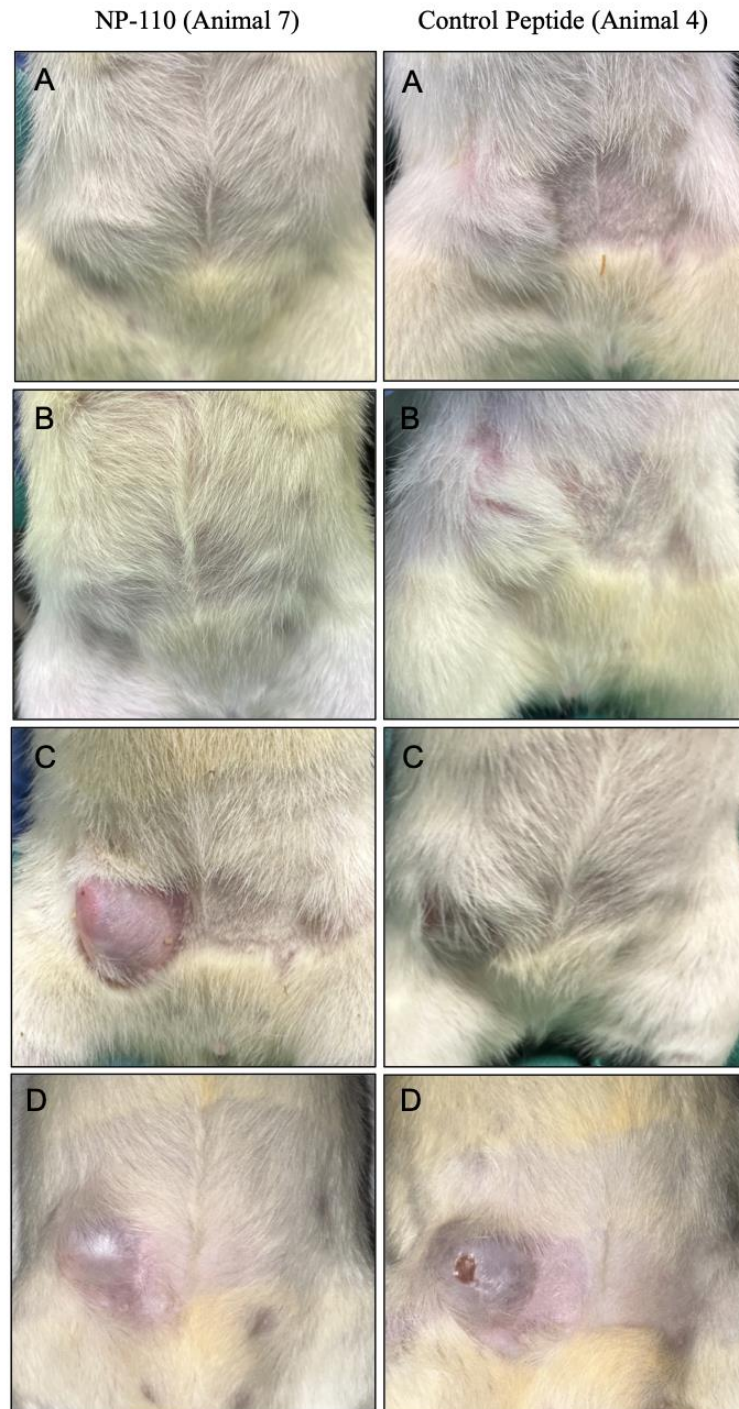


Figure 7. Implant site pre-radiation in animal 7 (NP-110) and 4 (control peptide) at A; one week post-radiation, B; two weeks post radiation, C; three weeks post radiation and D; four weeks post radiation (endpoint).

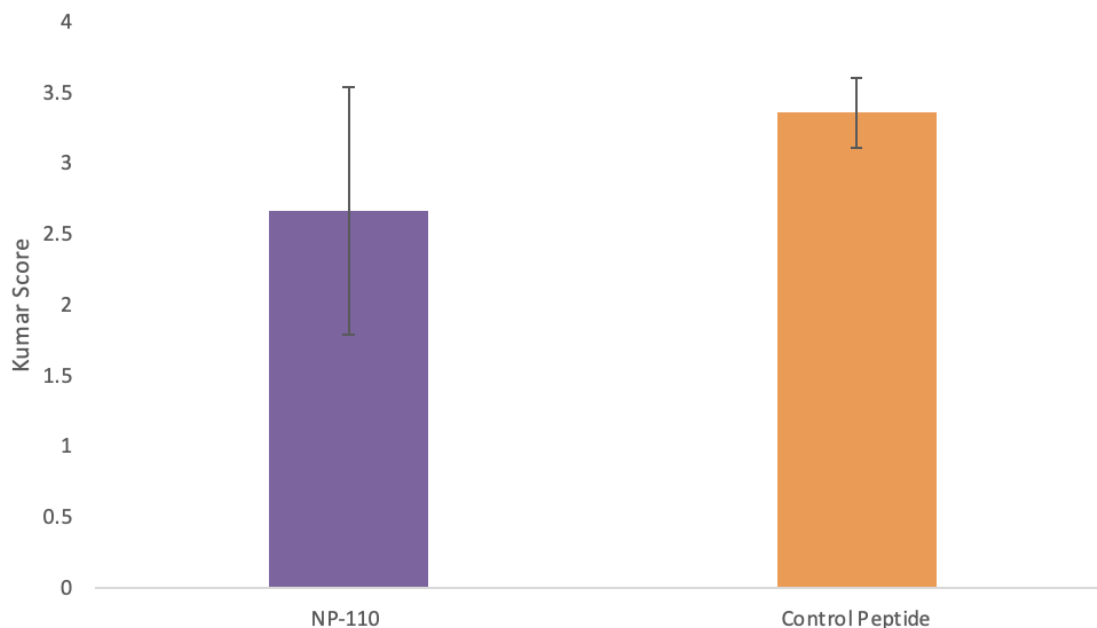


Figure 8. Average Kumar scores for animals in the NP-110 and control peptide groups at the end of the study period (4 weeks post-radiation), $p=0.462$ using Mann-Whitney U test.

4.2 Masson's Trichrome

The tissue was embedded with the implant in-situ. It was then removed, and the cavity filled with paraffin. This technique allowed the tissue architecture to be preserved and for the capsule to be easily visualized (Figure 9). As seen in Figure 9, decreased Masson's Trichrome blue staining were observed in the samples from the NP-110 treated group compared to control (Figure 9 & 10). This was evident in both low power images of the entire capsule as well in the high power (10X magnification) images where the thickness of the capsule can be clearly defined (Figure 10).

Quantification of blue stained pixels from Masson's Trichrome-stained slides in specifically selected capsule tissue using ImageJ software measured significantly lower staining in the NP-110 group, 107.23 mean gray value, compared to the control peptide, 174.93 ($p<0.001$) (Figure 11). The higher the mean grey value, the darker the pixels

stained in the sample, which can be measured from a range of 0-255. Therefore, when compared to the animals treated with the control peptide, those that received NP-110 went on to develop capsules with significantly less collagen.

Shapiro-Wilk analysis of the Masson's trichrome quantification data for both groups was non-significant, therefore indicating the data is normally distributed. Levene test for homogeneity was also non-significant for all groups. Therefore, analysis performed between the groups used was an independent two-tailed T-test.

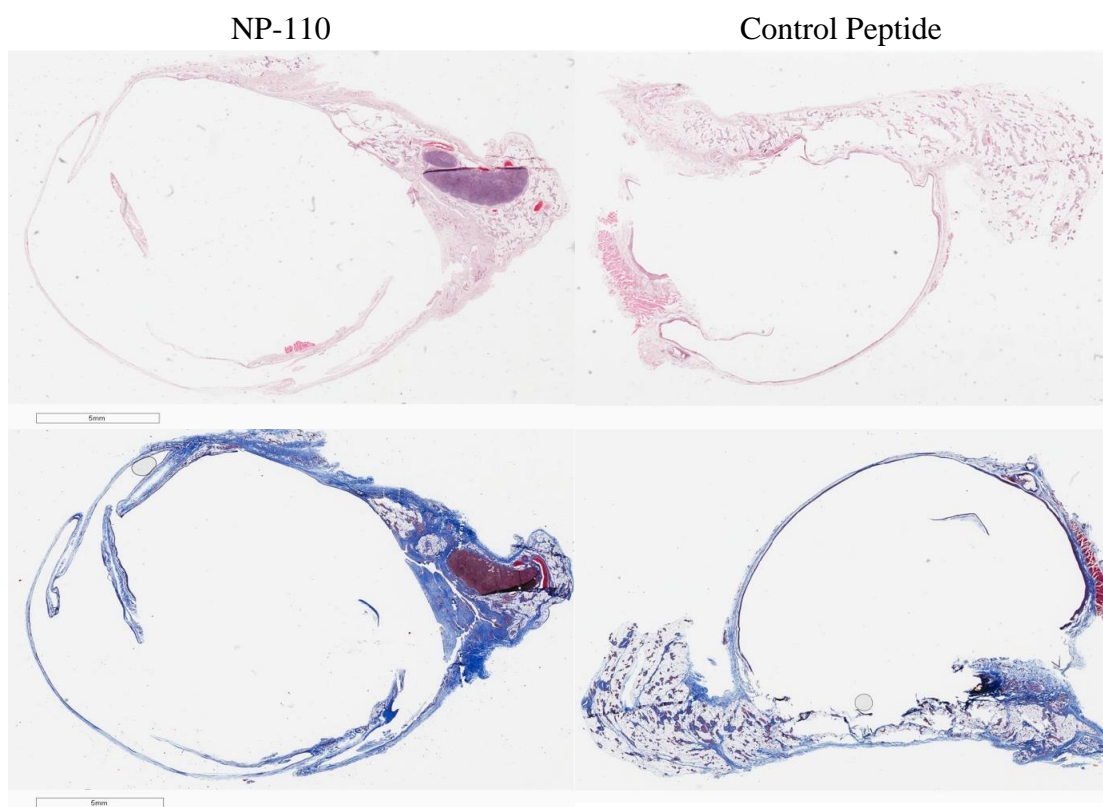


Figure 9. Representative images of paraffin embedded sections of entire capsule and fat pad specimen post sectioning from animal 1 from the NP-110 group (left) and animal 6 from the control peptide group (right). Stained with H&E (top) and Masson's trichrome (bottom).

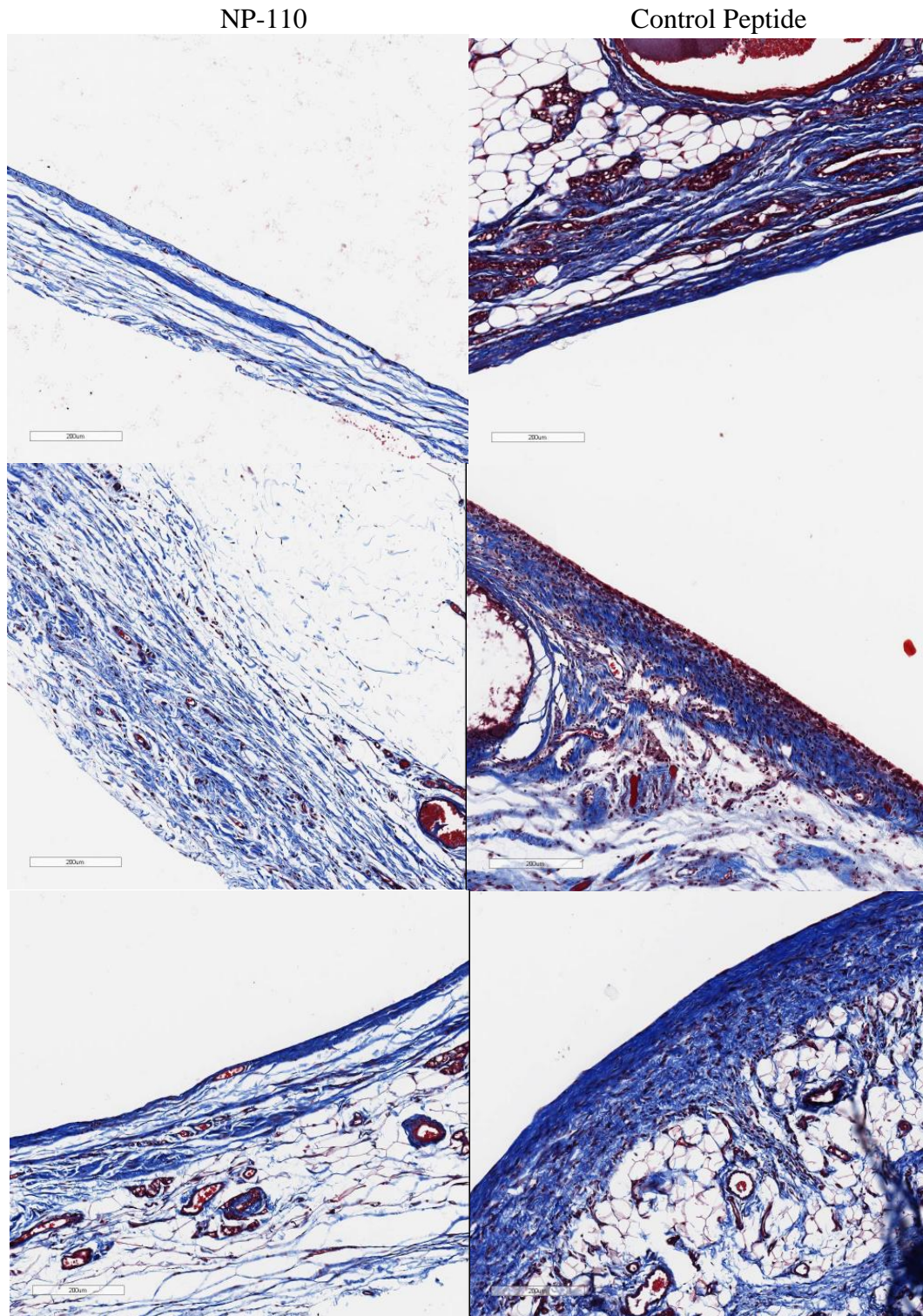


Figure 10. Representative images of implant capsule stained with Masson's Trichrome at 10X magnification. Capsules from the NP-110 group are thinner with less stain (left) compared to the control peptide groups (right).

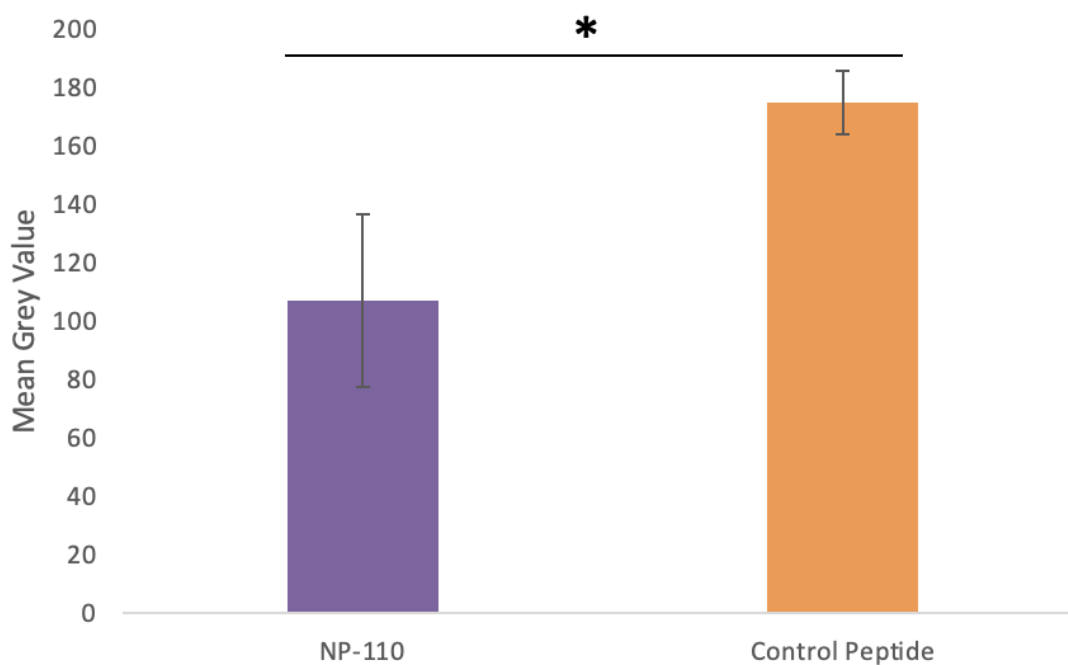


Figure 11. Mean grey value of capsule samples, selecting for blue Masson's trichrome staining for collagen using ImageJ software. Higher mean grey value indicates increased darkness of stain uptake from the sample and therefore increased collagen. There was significantly increased collagen stain in the control peptide group compared to the NP-110 group ($p=0.004$).

4.3 Picrosirius Red

Picrosirius red, under polarized light microscopy, detects collagen, with increased red staining indicating increased density of collagen bundling. The images from Picrosirius red staining, qualitatively appeared to have decreased red levels and decreased thickness of capsules from the NP-110 group compared to the control peptide group (Figure 12).

When measured quantitatively using ImageJ software, the NP-110 group had significantly lower percent area of red pixels in the capsule tissue, 11.62%, compared to

the control peptide group, 21.13% ($p < 0.001$) (Figure 13). Therefore, the animals that were treated with the NP-110 peptide immediately prior to radiation had less densely bundled collagen compared to the control peptide group.

Shapiro-Wilk analysis of Picrosirius red data from both groups were non-significant, therefore indicating the data is normally distributed. Levene test for homogeneity was also non-significant for all groups. Therefore, analysis performed between the groups used was an independent two-tailed T-test.

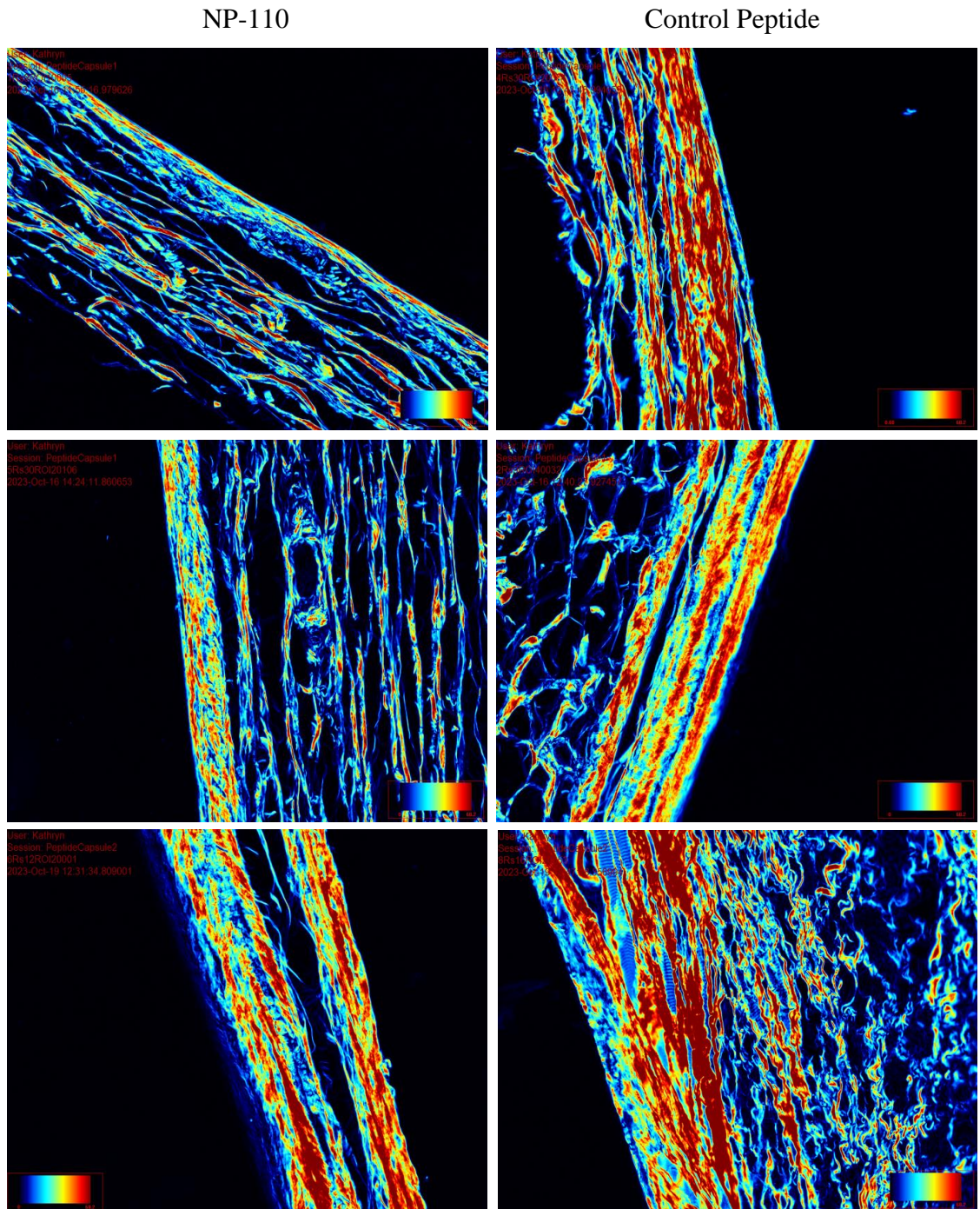


Figure 12. Representative images of implant capsule stained with Picrosirius red at 40X magnification. Capsules from the NP-110 group are thinner with less stain (left) compared to the control peptide groups (right).

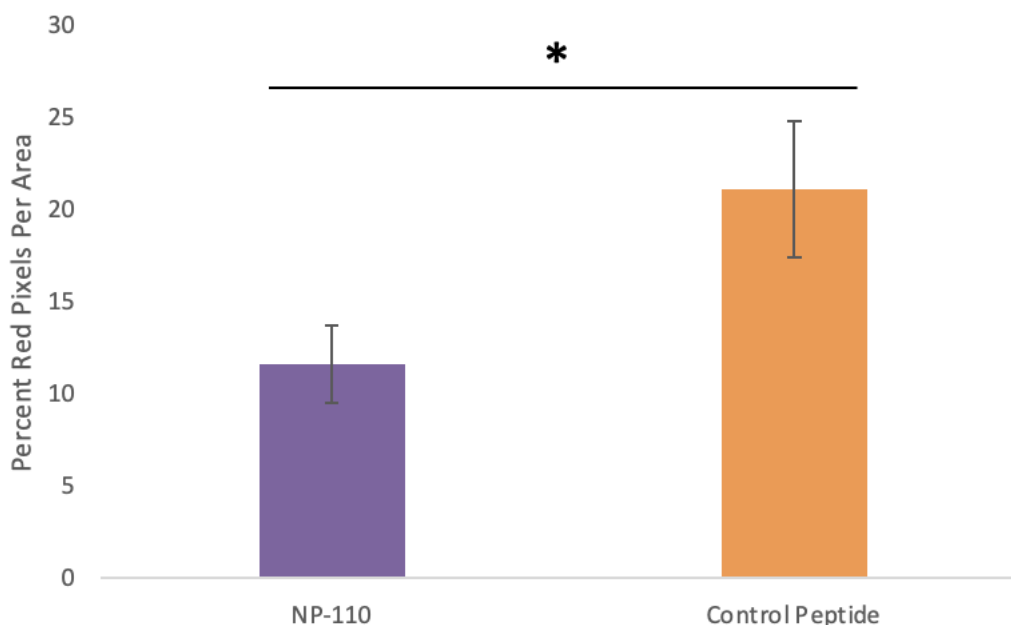


Figure 13. Percent of red pixels per area of capsule samples, selecting for area of the capsules using ImageJ software. Higher percent red pixels indicates increased Picrosirius red stain from the sample and therefore increased collagen deposition and bundling. There was significantly increased red staining in the control peptide group compared to the NP-110 group ($p < 0.001$) when calculated with an independent two-tailed T-test.

4.4 Hydroxyproline Assay

The hydroxyproline and total protein assays were completed using tissue scraped from 25 slides which include both the capsule and fat pad tissue from the specimen. The ratio of hydroxyproline (ug/well) to total protein (ug/well) in the sample was calculated which serves as a surrogate measurement of the ratio of collagen in the sample compared to other proteins in the tissue, and therefore a higher ratio indicates increased collagen levels in the sample. In the analysis, there was no significant difference between the NP-110 group with a ratio of 0.021, compared to the control group of 0.020 (Figure 14).

However, there was a high standard deviation in the NP-110 group of 0.007 compared to 0.002 for the control group.

Shapiro-Wilk analysis of all assay data were both non-significant, therefore indicating the data is normally distributed. However, the NP-110 group and control peptide group Levene test for homogeneity was significant. Therefore, a Mann-Whitney U test was used for any comparisons with these two groups.

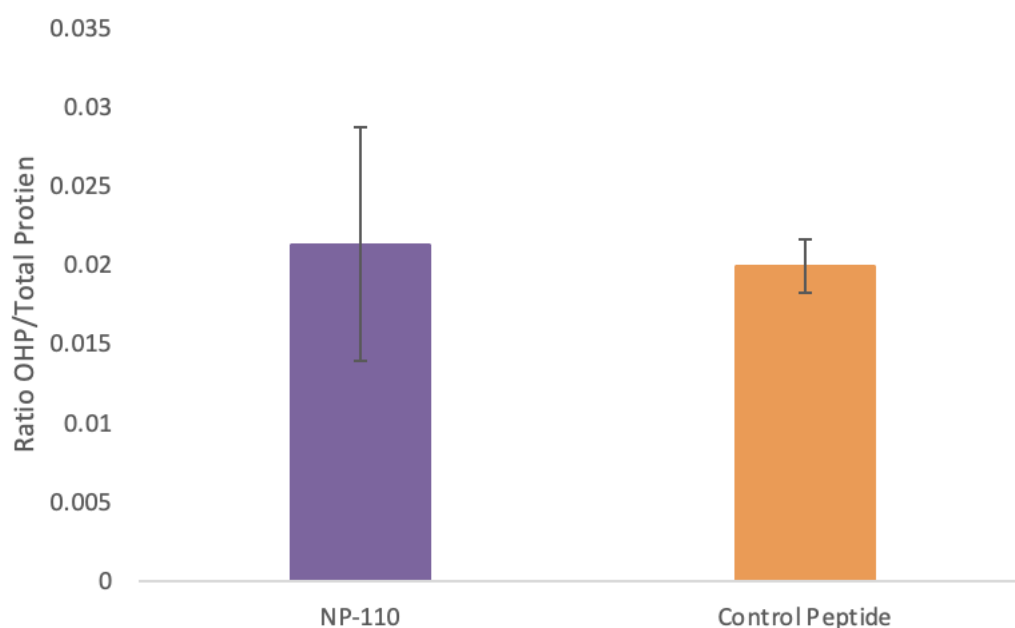


Figure 14. Ratio of the amount of total protein (ug/well) to hydroxyproline (ug/well) in the NP-110 and control peptide groups capsule + fat pad tissue. There was no significant difference between the NP-110 and control peptide groups ($p=0.652$).

4.5 Transforming Growth Factor Beta 1 (TGFB1)

Sections of capsule and adjacent fat pad tissue were stained for TGFB1 using immunofluorescence, which stains the protein of interest green, to evaluate the levels of this pro-inflammatory cytokine at the endpoint of the study. As seen in Figure 15, TGFB1 levels are increased in the capsular tissue compared to the surrounding tissue. When the amount of staining was quantified using ImageJ software, there was decreased staining in the NP-110 group compared to the control peptide group, however, this did not reach

statistical significance (Figure 16). When comparing the level of TGFB1 immunofluorescence in the mammary fat pad tissue, there was no significant difference between groups.

Shapiro-Wilk analysis of TGFB1 capsule and fat pad data were both non-significant, therefore indicating the data is normally distributed. However, the Levene test for homogeneity was significant for both the capsule and fat pad data sets. Therefore, a Mann-Whitney U test was used for any comparisons.

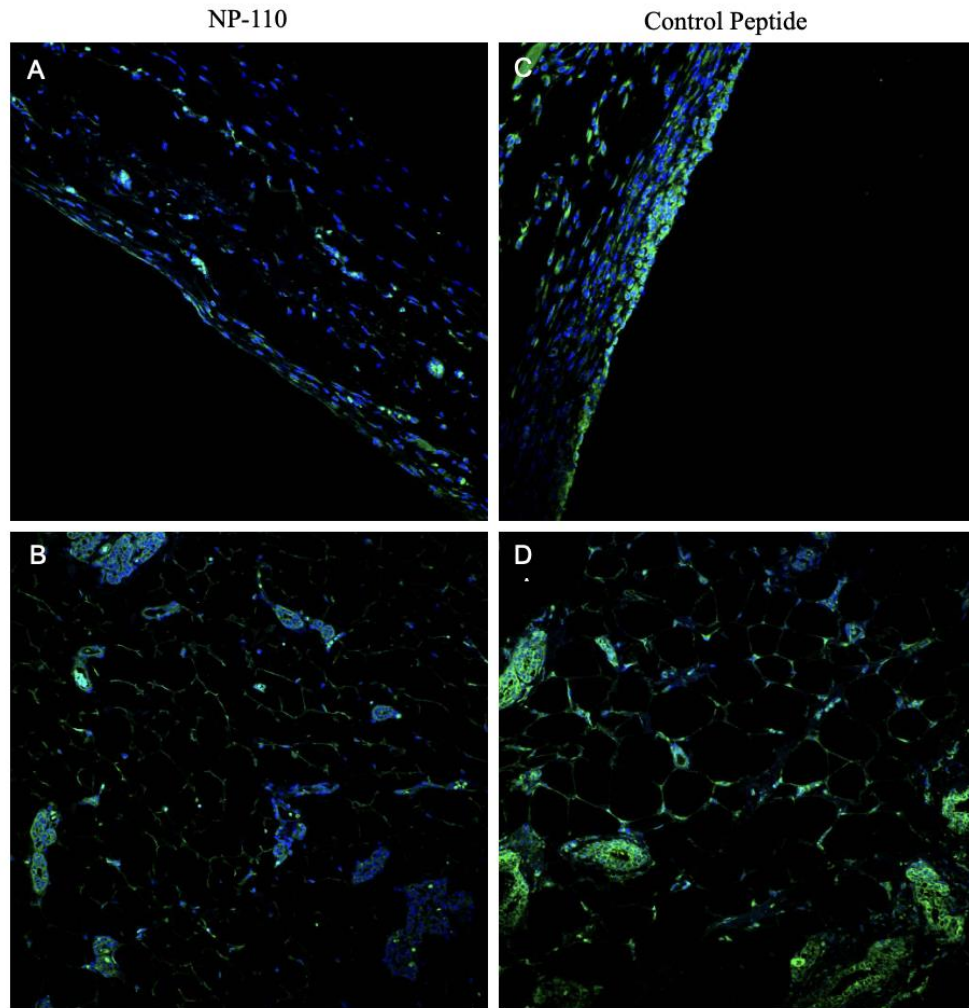


Figure 15. Representative images of TGFB1 immunofluorescence staining of the capsule tissue (A&C) and mammary fat pad (B&D) from an animal treated with NP-110 (A&B) and control peptide (C&D) at 40X magnification. TGFB1 is seen in green with DAPI to stain the nuclei blue.

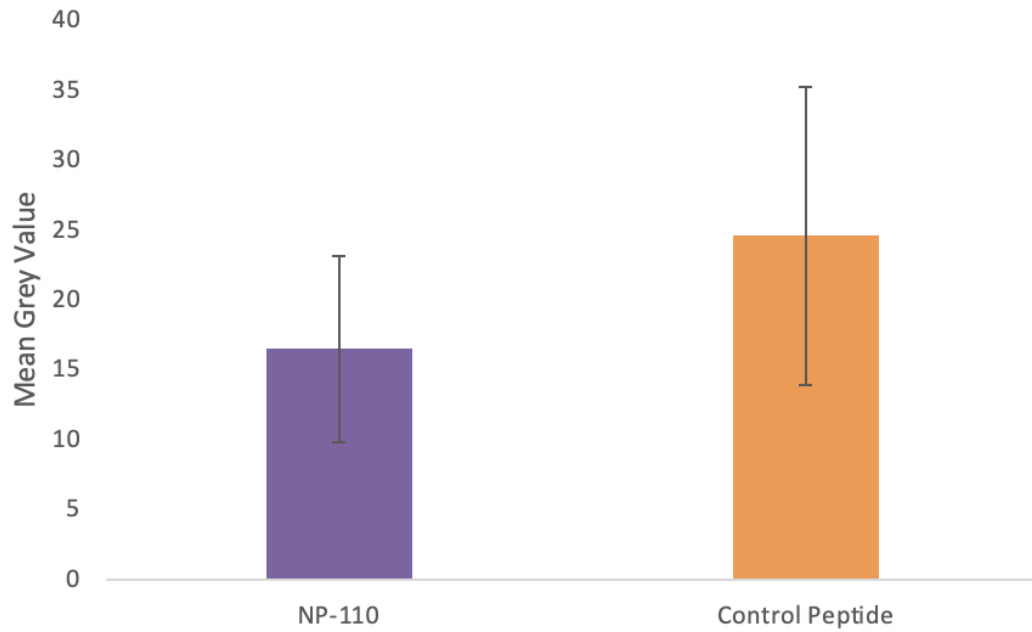


Figure 16. Mean grey value after selecting for green pixels in ImageJ from TGFB1 immunofluorescence of capsule tissue, $p=0.592$ using Mann Whitney U test.

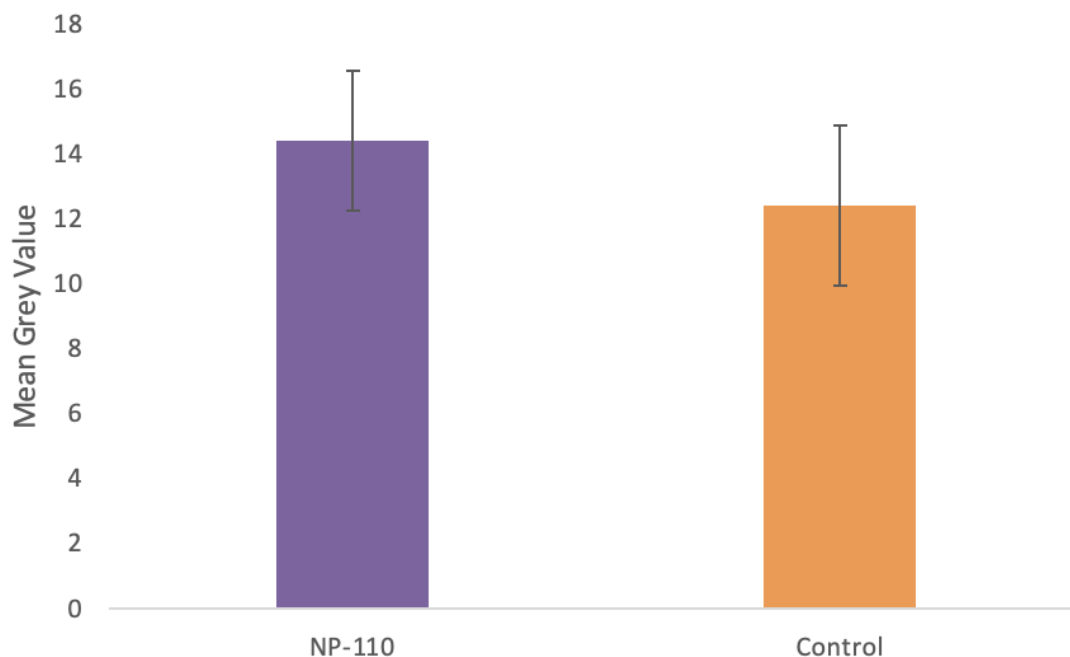


Figure 17. Mean grey value after selecting for green pixels in ImageJ from TGFB1 immunofluorescence-stained slides of mammary fat pad tissue, $p=0.286$ using Mann Whitney U test.

4.6 Alpha Smooth Muscle Actin (aSMA)

Sections of capsule tissue were stained for aSMA, a protein expressed by contractile myofibroblasts using immunofluorescence. As seen in Figure 18, aSMA levels are increased in the capsular tissue adjacent to the implant where the myofibroblasts are concentrated. When the amount of staining was quantified using ImageJ software, there was decreased staining in the NP-110 group compared to the control peptide group, however, this did not reach statistical significance (Figure 19).

Shapiro-Wilk analysis of aSMA data was non-significant, therefore indicating the data is normally distributed. However, the Levene test for homogeneity was significant. Therefore, a Mann-Whitney U test was used for any comparison between groups.

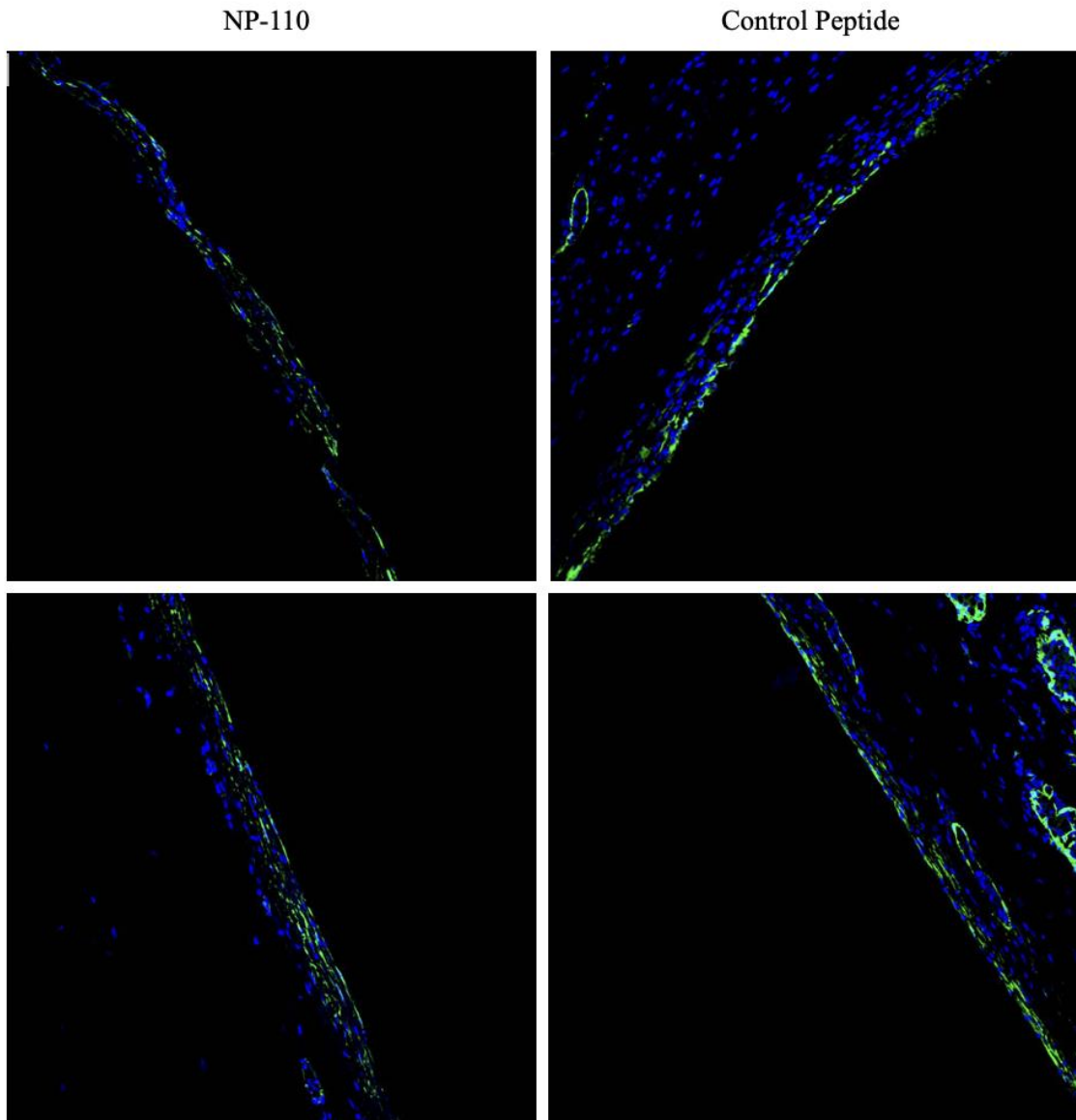


Figure 18. Representative images of aSMA immunofluorescence staining of the capsule tissue from NP-110 (left) and control peptide (right) treated animals at 40X magnification. aSMA is seen in green with DAPI to stain the nuclei blue.

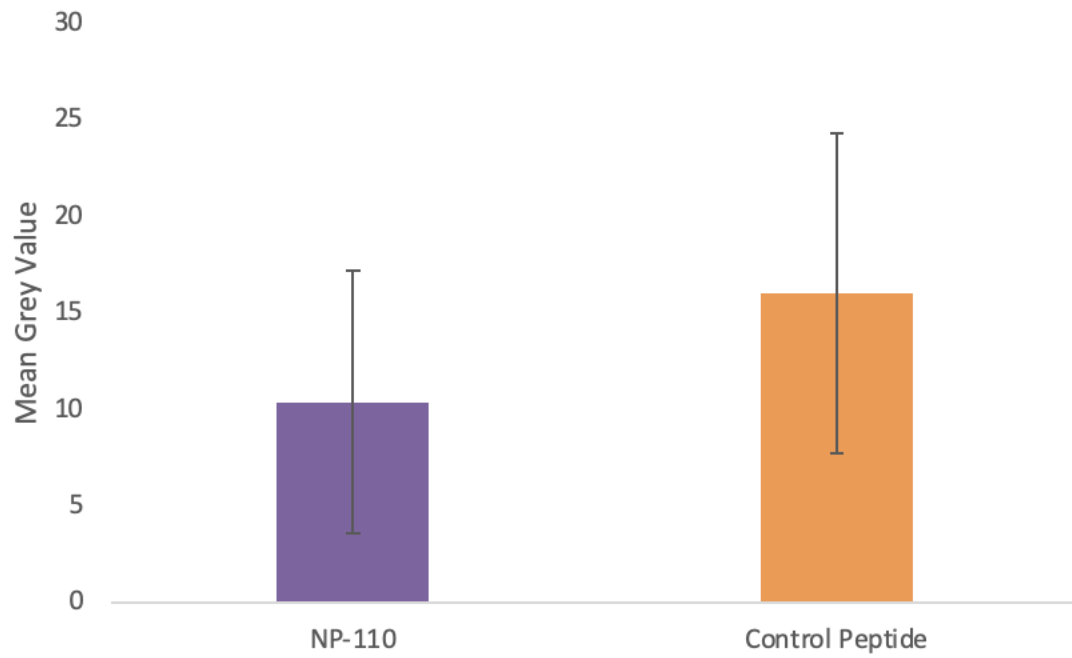


Figure 19. Mean grey value after selecting for green pixels in ImageJ from aSMA immunofluorescence of capsule tissue, $p=0.103$ using Mann Whitney U test.

Chapter 5

5 Discussion and Conclusion

The main objective of this thesis is to use the novel model for radiation-induced capsular contracture developed by T. DeLyzer *et al*, to evaluate the role of RHAMM in the development of capsule fibrosis using the RHAMM function-blocking peptide mimetic, NP-110. The role of RHAMM in the development of capsular contracture has not yet been elucidated. We aimed to identify if this pathway is playing a role in the pathogenesis of this common complication of implant-based breast reconstruction. We demonstrated that the rats treated with NP-110 scored lower on clinical assessment scales of radiation induced skin changes and capsule fibrosis. Furthermore, the capsules from the NP-110 treated group had significantly lower collagen deposition and less-dense bundling than the control peptide group on two histological stains. There was no significant difference in the NP-110 compared to control peptide groups for hydroxyproline analysis of both the capsule and fat pad tissue.

Overall, the use of NP-110 showed a reduction in capsule fibrosis in a novel model of radiation-induced implant capsular contracture. Therefore, these results provide evidence that the RHAMM pathway is involved in the pathogenesis that leads to capsule fibrosis. Overall, this identifies the RHAMM pathway as a potential target for non-surgical therapies to prevent or reduce capsular contracture.

5.1 Objective 1 Discussion

Replicate the previously developed rodent model for radiation-induced implant capsular contracture using the standardized procedures as outlined in the thesis work of T. DeLyzer et al. with the addition of injection of NP-110 or a scrambled control peptide to the mammary fat pad.

We followed the model outlined by DeLyzer *et al* with the addition of the peptide injection immediately prior to radiation⁵⁸. The model proved to be straightforward to replicate, with

the primary operator of this study being a junior surgical trainee (K. Minkhorst), compared to an experienced staff plastic surgeon (T. DeLyzer). Despite this, the surgery time remained low, of around 15 to 20 minutes of operative time, and an overall time of 35 to 45 minutes including induction and recovery of each animal. The operative procedure was set up with two assistants, (T. DeLyzer and N. Lewandoski), one as an operative assistant and the other who documented and observed the animals during recovery to allow for continuing to the next animal as the previous one recovered. Overall, all animals in the study were able to be operated on two morning sessions making this quite reasonable for investigators and animal facility resources.

The timing and method of peptide injection was decided on for both practical reasons and based on previous study. Truong *et al* also used a one time of 100ug of NP-110 peptide and found significant reduction in the radiation-induced fibrosis of rodent mammary fat pads, which became the rationale for the dosing in this study⁵⁴. One difference was that we did not inject at post-radiation day 1, but instead immediately prior to radiation. This was chosen as the animals were already under anesthesia for the radiation protocol, and this reduced the need for a separate induction and anesthetic exposure for the peptide injection, reducing the risk of harm to the animals and reducing time and resource requirements for the investigators. Furthermore, the injections were done by landmarking to the right 4th nipple and performing a subcutaneous injection, which was not confirmed by ultrasound guidance as done by Truong *et al*⁵⁴. Despite this change, our study still showed a significant reduction in capsule fibrosis in the NP-110 group, suggesting our dosage, timing, and delivery method were effective. By eliminating the use of ultrasound guidance we simplified the protocol to make it more accessible to other researchers for replication, and in the clinical setting, that a simple subcutaneous injection may be an appropriate delivery method.

The radiation protocol for this study was modified slightly from DeLyzer *et al*, as the unit that was used in their study was no longer in service at our institution. Instead, we used a clinically active Orthovoltage unit, to deliver a 26Gy dose of ionizing radiation in a single session. Despite this change, we did still see significant radiation changes clinically and histologically. Previous models of radiation induced capsular contracture have used doses

ranging from 10Gy to 35Gy, to varying degrees of capsule fibrosis and harm to the experimental animals^{37,55,56,58}. In our teams experience, both in the development of Troung *et al* and DeLyzer *et al* models, the 26Gy dose was sufficient in producing significant radiation-induced fibrosis without systemic illness in the experimental rats.

Finally, we used the timeline devised by DeLyzer *et al* of radiation four weeks post-operatively and the endpoint of the study four weeks post radiation⁵⁸. This timepoint was chosen based on the rat lifespan, which is approximately 3 years, with one human year being the equivalent of two to six weeks⁶¹. Most patients who undergo breast reconstruction with implants develop capsular contracture within a year post-surgery or post-radiation^{3,5}. Previous animal models have also shown significant changes in the implant capsules by post-radiation week three²⁰. Therefore, this timeline has been proven to be sufficient to show significant change in the implant capsules post-radiation, while still allowing for researchers to conduct studies in a timely fashion.

5.1.1 Conclusions and Limitations of Objective 1

The overall goal for the first objective of this thesis was to replicate the previously developed model of radiation-induced implant capsular contracture with the addition of an experimental agent. The previously developed model proved easy to replicate and therefore further enforces the previous work of DeLyzer *et al* that this model is an effective tool in the study of capsular contracture. The efficiency of the team was supported by the fact that the main operator (K. Minkhorst) was the primary assistant in the previous experiments, however, there was an interval of two years between the previous study and the current thesis work. Therefore, it is concluded that the procedure is straightforward and easily replicable, especially considering it was easily completed by a junior surgical trainee (K. Minkhorst) although developed by an experienced staff plastic surgeon (T. DeLyzer).

This model was developed by DeLyzer *et al*, and has the advantage of mimicking the location of the implant in the mammary region instead of other models which typically place the implant dorsally^{30,37,56}. This provides the implant with a similar microenvironment of the location of implant placement in patients, however there still are some important differences. Firstly, we did not remove the mammary fat pad, which would

not mimic the post-mastectomy tissue trauma in this patient population. Secondly, typically in implant-based reconstruction the implant is placed sub-pectoral with acellular dermal matrices to support the implant³⁴. There are some animal models that use other anatomic areas to mimic the submuscular placement, such as under the latissimus dorsi muscle³⁰. However, as it is the dorsal region with no nipple, or other relevant structures, it is not a perfect model either. Researchers must choose to make compromises in their model choice as the abdomen musculature cannot be used to make a sub-muscular pocket as the implant would then be intra-peritoneal. For the purpose of this thesis, we chose to prioritize the mammary tissue-microenvironment over the sub-muscular implant placement. Therefore, the current model is a useful addition to those that exist, as it helps to increase the overall knowledge of capsular contracture pathogenesis.

Another limitation of this work is the use of a different radiation unit from the protocol described by DeLyzer *et al* and our current study. We used a clinically active Orthovoltage unit designed for radiating skin cancers primarily, whereas in the previous project a decommissioned clinical linear accelerator that was designated for research use was used. This could have affected the penetrance of the radiation, as orthovoltage units are typically used to treat superficial cancers, such as skin cancer, due to their decreased penetration into the tissue compared to linear accelerators⁶². This may explain why the animals in our study did have more hair loss and skin changes compared to the previous study⁵⁸. However, as the implant and fat pad are superficial structures in the rodent abdomen, and we saw significant fibrosis in our experiments, we can conclude that the dose of 26Gy from orthovoltage radiation is sufficient to induce capsular contracture in this model. Additionally, this finding may provide reassurance to other researchers that they can use this model with whichever radiation unit their institution has available, either a linear accelerator or an orthovoltage unit, will still produce measurable capsule fibrosis.

5.2 Objective 2 Discussion

Evaluate the effect of local NP-110 injection into the mammary fat pad tissue on implant radiation-induced capsule fibrosis compared to an inactive control peptide, radiation alone, and non-radiated capsules.

Qualitatively, we saw an increase in capsule fibrosis as well as radiation induced skin changes in all animals post-radiation. This effect was somewhat reduced in the NP-110 group compared to the control peptide. Similarly to the results seen from Truong *et al* and DeLyzer *et al*, the skin changes were relatively mild and no systemic injury from radiation to the animal was observed^{54,58}. All of the animals in our study did develop at least grade 2 implant capsular contracture, with all the animals in the control group developing grade 3 contracture. Although this scale was developed for human patients with implants, the decreased mobility of the implant and increased implant visibility are hallmark features of capsular contracture³. Therefore, the inclusion of this qualitative evaluation of the implants and capsules in our study provides some insight into what the effect of NP-110 treatment may translate to clinically for patients, although more studies are needed.

Quantitatively, using Masson's trichrome and Picrosirius analysis of capsule tissue, there was significantly decreased collagen deposition and bundling in the NP-110 treated group compared to the control peptide. Interestingly, when compared to the previous data from DeLyzer *et al*, with the Masson's trichrome analysis there was no significant difference between the NP-110 treated capsules and the non-radiated capsules (Appendix 1)⁵⁸. This result is significant, as it shows that treatment with NP-110 not only decreases fibrosis compared to other radiated capsules, but the degree in which it prevents fibrosis is similar to capsules that had not been radiated. Similarly, for the Picrosirius analysis, there was significantly lower red staining, and therefore collagen bundling in the NP-110 group compared to the groups treated with the control peptide ($p < 0.001$) and the group that received radiation alone from DeLyzer *et al* previous study (Appendix 2). We re-analyzed the images from the previous study, using the polygon function in ImageJ and select for only capsule tissue. This was done for both the current and previous study in order to control for the variability of capsule tissue, especially from DeLyzer *et al* slides as an outside lab performed the image capture and there was significant variability in the

regions of interest. In the current study, we performed the image capture as COVID-19 restrictions were lifted, which allowed for more consistency between regions of interest captured. Although these results are in an animal model, both the Masson's Trichome and Picrosirius red staining are consistent that NP-110 resulted in capsules with decreased collagen deposition and bundling of collagen fibers, compared to both those treated with the control peptide and radiation alone. Therefore, we have also shown that the scrambled control peptide has no activity and the NP-110 peptide which blocks RHAMM signaling is the agent resulting in decreased capsule fibrosis. Furthermore, the dose of peptide used in this study was adequate to prevent capsule fibrosis to a degree that these NP-110 treated capsules were similar to those that had not been radiated. This result reinforces the importance of RHAAM as a target for prevention of capsular contracture.

RHAMM has been implicated in a number of pro-fibrotic processes, and the RHAMM signaling pathway is a regulator in fibroblast migration and wound repair^{47,48,50}. Fibroblasts and myofibroblasts are abundant in implant capsule tissue, and overactivity of these cells are believed to be implicated in the pathogenesis of capsular contracture³⁶. Although other studies have looked at capsule thickness, we wanted to assess not only amount of collagen in the implant capsules but the degree of collagen bundling⁵⁵. In human samples from capsular contracture patients, the capsules are not only thicker but tighter around the implant, and squeeze down on the prosthesis, causing discomfort and disfigurement³⁴. When there is increased collagen cross-linking, the strength of this tissue layer increases and therefore decreases the mobility of the implant⁵¹. Our study shows that not only does RHAMM function-blocking peptide mimetic NP-110 reduce the collagen deposition, but also decreases collagen bundling in the capsule. This is consistent with previous study of radiation-induced fibrosis of rat mammary fat pads⁵⁴. In their study, Truong *et al* showed that NP-110 increased collagen 3 mRNA expression, indicating that RHAMM is involved in the regulation of collagen deposition and bundling⁵⁴. Increased expression of collagen 3 isoforms has been shown to reduce tissue rigidity, compared to increased expression of collagen 1 isoforms which is associated with increased tissue rigidity and fibrosis^{63,64}. Future study using this model is needed to analyze the expression of fibrogenic mRNA and better characterize the effect of NP-110 on the capsule and surrounding tissue microenvironment.

We measured TGFB1 levels in the capsule tissue and the adjacent mammary fat pad using immunofluorescence. TGFB1 levels were not significantly decreased in the capsule tissue from NP-110 treated animals compared to control. There was no significant difference between the groups in level of TGFB staining in the mammary fat pad. Truong *et al* measured TGFB1 levels in their rat model of radiated mammary fat pads using qPCR, there was an increase in expression of TGFB1 after radiation that was decreased in animals treated with RHAMM function blocking peptides versus control, although this decrease was not significant⁵⁴. However, the specimens were from three weeks post-radiation, and previous work has shown that TGFB1 expression peaks within the first week of radiation exposure^{18,65}. Similarly, our specimens were from four weeks post radiation, and the peak of TGFB1 expression may have passed at that point, leading to the lack of significance in this result. Therefore, we hypothesize that there may be a link between TGFB1 signaling and RHAMM in radiation-induced fibrosis and the development of capsular contracture, although further experimentation is needed to better elucidate these pathways.

TGFB1 has been identified as a key cytokine in the promotion of myofibroblast differentiation and survival¹⁸. In radiation tissue injury, TGFB1 is upregulated in the extracellular matrix within hours of ionizing radiation exposure^{65,66}. In a mouse model of radiation induced fibrosis, animals were treated with ionizing radiation to the hind leg, and those given a TGFB inhibitor had significantly decreased tissue fibrosis seen on Masson's trichrome staining compared to control¹⁹. Furthermore, in a model of radiation induced capsular contracture with Smad3 knockout mice, which is a protein downstream in the TGFB pathway that is activated by the TGFB1 receptor, decreased capsule thickness and fibrosis was seen in the animals missing this downstream protein compared to controls²⁰. In cell tissue culture, increased RHAMM protein was detected on the cell surface after stimulation with TGFB1, and the effect of TGFB1 induced cell locomotion was reduced by antibodies that inhibited RHAMM signaling⁶⁷. Future study could aim to analyze TGFB expression in the capsule and fat pad tissue at various time points post-radiation to better elucidate the link between NP-110 and its effect on this pro-inflammatory cytokine in the setting of capsule fibrosis.

Similar to the findings with TGF β 1, immunofluorescence staining for α SMA was increased in the control peptide treated capsules compared to control, however was not statistically significant. Myofibroblasts express α SMA, and increased levels of this protein in the cells has been linked to increased contractility⁶⁸. Furthermore, exposure to TGF β 1 increases the expression of α SMA in fibroblast cell culture⁶⁸. Therefore, the increase in myofibroblasts, and therefore contractility of the capsule around the implant may be influenced by local inflammation and TGF β 1 expression^{51,68}. Similar to previous studies, we showed expression of α SMA in capsular tissue, which was slightly decreased by treatment with NP-110^{7,51}. This finding validates that the composition of capsular tissue in our animal model is similar to histological samples from human capsular tissue, and that myofibroblasts are predominate cells among the collagen fibrils⁵¹. Although we did not see a statically significant difference in our sample, there was high level of variance, likely due to the heterogenous expression of myofibroblasts throughout the capsules, and therefore a larger sample size may be required to reach statistical significance.

The hydroxyproline to total protein ratio in the NP-110 treated capsule and fat pad tissue was not significantly different compared to the control peptide group. This result differed from the previous work from DeLyzer *et al*, where an increase in the hydroxyproline was seen in the radiated group compared to control(Figure 20)⁵⁸. One explanation for this result is that between the completion of the previous study and our current experiments, Biovision changed the formulation of their hydroxyproline assay, which could affect the accuracy of this test. Indeed, we did see an increase in the standard deviation of the samples, especially in the NP-110 group. Furthermore, this test uses tissue scrapped from paraffin slides that included the fat pad and capsule tissue. There was a differing amounts of fat pad tissue present on the slides due to inconsistency in tissue orientation and sectioning, that could have increased variability in our sample. For this reason, utilizing a different method of evaluating the effect of NP-110 on the capsule and fat pad tissue level of collagen in the future may provide more conclusive results.

5.2.1 Conclusions and Limitations of Objective 2

Overall, the experiments conducted in this study provide evidence that the use of RHAMM function blocking peptide, NP-110, significantly decreases radiation-induced capsule fibrosis. Therefore, we conclude that the RHAMM signaling pathway may be implicated in the development of capsular contracture, and is a target for development of possible therapeutic agents.

Limitations of these include the lack of mRNA expression analysis to characterize the change in transcription as a result of NP-110 treatment. Unfortunately, to preserve the tissue architecture in our tissue processing and paraffin embedding we did not have any tissue available for western blot or qPCR analysis. In the previous work by DeLyzer *et al*, some of the capsule and fat pad sections were bisected and saved in the -80 degree Celsius freezer, however the slides from these samples were much more difficult to orient and assess the capsule tissue compared to the method used in our current study⁵⁸. The hydroxyproline tissue assay was in part chosen for these studies because they could be done using tissue scraped from the paraffin slides. However, as seen in this study there was no significant difference between the NP-110 group and the control, and significant variability in the samples. This could be resolved by increasing the number of technical replicates to increase the accuracy of this test as well as possibly increase the sample size of the animals in each treatment arms. Future experiments could include animals that were euthanized at various time points to assess the effect of NP-110 on the tissue microenvironment and transcriptome at various time points using other experimental techniques.

Furthermore, although there have been previous studies that have shown a significant effect of using NP-110 in a radiation model, there is no specific work looking at the stability of NP-110 post-radiation⁵⁴. Therefore, it is possible there was some effect of the radiation on NP-110 and we did not measure NP-110 levels in the tissue post-radiation. However, there is the advantage of mimicking the possible timing and delivery of what could be done clinically. Therefore, since we did still see a significant effect on the capsule fibrosis of the animals treated with NP-110 we can hypothesize it is able to have some stability and effect post-radiation. It would be useful in future studies to test the

stability of NP-110 after radiation to better understand the feasibility of using peptide mimetics for possible prevention of capsular contracture.

Lastly, in this protocol we only delivered a one-time dose of 100ug of NP-110 peptide. The dose of 100ug once was based on the results of Truong *et al* which found this dose effective in reducing radiation induced mammary fat pad fibrosis⁵⁴. However, other studies have used weight-based dosing of NP-110 (3mg/kg) at multiple time points, in a murine model of bleomycin-induced scleroderma⁵³. Although our results were significant, it would be interesting to explore the effect of variable doses, as well as repeat delivery of peptide to evaluate the effect of NP-110 more rigorously.

5.3 Significance and Future Directions

To our knowledge, this study is the first evaluation of the effect of NP-110 on implant capsule fibrosis in a novel rodent model of radiation-induced capsular contracture. This work builds upon previous studies in the Turley lab on the impact of RHAMM function blocking peptides on rat mammary fat pad fibrosis. Both this previous work and our study show that the use of NP-110 reduces radiation-induced fibrosis in a rat model⁵⁴. Therefore, the RHAMM pathway is implicated in the pro-fibrotic process of radiation-induced capsule fibrosis. The pathogenesis of capsular contracture is not fully understood, and this study provides evidence that HA fragmentation and activation of RHAMM may be involved, identifying new targets for study and possible non-surgical therapeutic development.

Capsular contracture is a common and unpredictable complication in patients who undergo implant-based breast reconstruction post-mastectomy, especially in the context of radiation therapy^{1,5,11,34}. Animal models have implicated TGFB1 and SMAD signaling pathways in development of capsule fibrosis, however the underlying molecular mechanism is not fully understood^{19,20}. Furthermore, due to the ubiquitous action of these pathways, they may not be ideal targets for the treatment or prevention of capsular contracture⁶⁵. Therefore, the evidence that RHAMM function blocking peptide (NP-110), decreases capsule fibrosis adds to the literature a potential new therapeutic target for the prevention of capsular

contracture. We have also shown that local delivery of this peptide is possible via injection into the mammary tissue using only surface landmarks and therefore is easy and quick to deliver. However, injection of a peptide clinically may pose barriers to patient treatment in the future, for concerns of pain, sterility and potential damage to the underlying implant. Therefore, other routes of administration of RHAMM peptide mimetics could be investigated for feasibility and effect.

Lastly, there is much interest in the role of ADSCs in the treatment of capsular contracture, and fat grafting has become a common adjunct in breast reconstruction surgery^{5,32}. However, there is variable survival of the fat graft in these tissues³². The use of RHAMM function blocking peptide mimetics has been shown to increase adipogenesis in a rat model of mammary fat pad radiation induced fibrosis⁵⁴. Therefore, it would be valuable to study the use of fat graft together with RHAMM function blocking peptides, as these two therapies may work synergistically to decrease tissue fibrosis and increase fat survival, increasing efficacy of fat grafting surgery.

5.4 Conclusion

In conclusion, the investigation outlined in this thesis has provided valuable insights into the role of RHAMM in radiation-induced capsular contracture and has laid the groundwork for potential non-surgical therapies to mitigate this common complication of implant-based breast reconstruction. Through the replication of the rodent model for radiation-induced capsular contracture and the evaluation of the effect of NP-110, several significant findings have emerged.

Firstly, the replication of the rodent model demonstrated the feasibility and reproducibility of the experimental setup, even when conducted by a junior surgical trainee. The slight modification in the radiation protocol, utilizing a clinically active Orthovoltage unit, did not hinder the induction of significant radiation-induced fibrosis, affirming the robustness of the model. Additionally, the timing and method of peptide injection were optimized for practicality and efficacy, simplifying the protocol for future studies.

Secondly, the evaluation of NP-110's effect revealed promising results. Qualitatively, a reduction in capsule fibrosis and radiation-induced skin changes was observed in the NP-110 group compared to the control peptide group. Quantitative analyses further supported these findings, demonstrating significantly decreased collagen deposition and bundling in the NP-110 treated capsules. Importantly, NP-110 treatment maintained capsules similar to non-radiated ones histologically, suggesting its potential to prevent fibrosis.

However, certain limitations need to be addressed. The lack of mRNA expression analysis and variability in the hydroxyproline assay results underscore the need for further experimentation to elucidate NP-110's mechanisms of action conclusively. Moreover, exploring variable doses and repeat delivery of NP-110 could provide deeper insights into its therapeutic potential.

Despite these limitations, the study holds significant implications for future research and clinical applications. The identification of RHAMM function-blocking peptide mimetics as promising therapeutic agents for preventing capsular contracture opens avenues for novel treatment modalities.

In conclusion, the findings presented in this thesis contribute to our understanding of capsular contracture pathogenesis and offer promising prospects for the development of effective non-surgical interventions. Through continued research and innovation, the goal of mitigating the burden of capsular contracture for breast reconstruction patients may soon become a reality.

References

1. Luvsannyam E, Patel D, Hassan Z, Nukala S, Somagutta MR, Hamid P. Overview of Risk Factors and Prevention of Capsular Contracture Following Implant-Based Breast Reconstruction and Cosmetic Surgery: A Systematic Review. *Cureus*. 12(9):e10341. doi:10.7759/cureus.10341
2. Magill LJ, Robertson FP, Jell G, Mosahebi A, Keshtgar M. Determining the outcomes of post-mastectomy radiation therapy delivered to the definitive implant in patients undergoing one- and two-stage implant-based breast reconstruction: A systematic review and meta-analysis. *Journal of Plastic, Reconstructive & Aesthetic Surgery*. 2017;70(10):1329-1335. doi:10.1016/j.bjps.2017.05.057
3. Safran T, Nepon H, Chu CK, et al. Current Concepts in Capsular Contracture: Pathophysiology, Prevention, and Management. *Semin Plast Surg*. 2021;35(03):189-197. doi:10.1055/s-0041-1731793
4. Spear SL, Baker JL. Classification of capsular contracture after prosthetic breast reconstruction. *Plast Reconstr Surg*. 1995;96(5):1119-1123; discussion 1124.
5. Haran O, Bracha G, Tiosano A, et al. Postirradiation Capsular Contracture in Implant-Based Breast Reconstruction: Management and Outcome. *Plastic and Reconstructive Surgery*. 2021;147(1):11. doi:10.1097/PRS.00000000000007453
6. Guimier E, Carson L, David B, Lambert JM, Heery E, Malcolm RK. Pharmacological Approaches for the Prevention of Breast Implant Capsular Contracture. *Journal of Surgical Research*. 2022;280:129-150. doi:10.1016/j.jss.2022.06.073
7. Hwang K, Sim HB, Huan F, Kim DJ. Myofibroblasts and Capsular Tissue Tension in Breast Capsular Contracture. *Aesth Plast Surg*. 2010;34(6):716-721. doi:10.1007/s00266-010-9532-8
8. Yun JH, Diaz R, Orman AG. Breast Reconstruction and Radiation Therapy. *Cancer Control*. 2018;25(1):1073274818795489. doi:10.1177/1073274818795489
9. Ribuffo D, Lo Torto F, Giannitelli SM, et al. The effect of post-mastectomy radiation therapy on breast implants: Unveiling biomaterial alterations with potential implications on capsular contracture. *Materials Science and Engineering: C*. 2015;57:338-343. doi:10.1016/j.msec.2015.07.015
10. Momoh AO, Colakoglu S, Westvik TS, et al. Analysis of complications and patient satisfaction in pedicled transverse rectus abdominis myocutaneous and deep inferior epigastric perforator flap breast reconstruction. *Ann Plast Surg*. 2012;69(1):19-23.
11. El-Diwany M, Giot JP, Hébert MJ, Danino AM. Delaying implant-based mammary reconstruction after radiotherapy does not decrease capsular contracture: An in vitro

- study. *Journal of Plastic, Reconstructive & Aesthetic Surgery*. 2017;70(9):1210-1217. doi:10.1016/j.bjps.2017.06.012
12. Barcellos-Hoff MH. The radiobiology of TGF β . *Seminars in Cancer Biology*. 2022;86:857-867. doi:10.1016/j.semcancer.2022.02.001
 13. Cagli B, Morelli Coppola M, Augelli F, et al. Postmastectomy Radiation Therapy in the Setting of Two-Stage Retropectoral Implant-Based Breast Reconstruction: Should It be Delivered Before or After Implant Exchange? A Retrospective Analysis on 183 Patients. *Aesth Plast Surg*. 2022;46(6):2643-2654. doi:10.1007/s00266-022-03001-7
 14. Wong JS, Uno H, Tramontano A, et al. Patient-Reported and Toxicity Results from the FABREC Study: A Multicenter Randomized Trial of Hypofractionated vs. Conventionally-Fractionated Postmastectomy Radiation Therapy after Implant-Based Reconstruction. *International Journal of Radiation Oncology, Biology, Physics*. 2023;117(4):e3-e4. doi:10.1016/j.ijrobp.2023.08.029
 15. Tang H, He Y, Liang Z, Li J, Dong Z, Liao Y. The therapeutic effect of adipose-derived stem cells on soft tissue injury after radiotherapy and their value for breast reconstruction. *Stem Cell Res Ther*. 2022;13(1):493. doi:10.1186/s13287-022-02952-7
 16. Ejaz A, Greenberger JS, Rubin PJ. Understanding the mechanism of radiation induced fibrosis and therapy options. *Pharmacology & Therapeutics*. 2019;204:107399. doi:10.1016/j.pharmthera.2019.107399
 17. Li MO, Wan YY, Sanjabi S, Robertson AKL, Flavell RA. Transforming growth factor-beta regulation of immune responses. *Annu Rev Immunol*. 2006;24:99-146. doi:10.1146/annurev.immunol.24.021605.090737
 18. de Andrade CBV, Ramos IPR, de Moraes ACN, et al. Radiotherapy-Induced Skin Reactions Induce Fibrosis Mediated by TGF- β 1 Cytokine. *Dose Response*. 2017;15(2):1559325817705019. doi:10.1177/1559325817705019
 19. Gans I, El Abiad JM, James AW, Levin AS, Morris CD. Administration of TGF- β Inhibitor Mitigates Radiation-induced Fibrosis in a Mouse Model. *Clin Orthop Relat Res*. 2021;479(3):468-474. doi:10.1097/CORR.0000000000001286
 20. Katzel EB, Koltz PF, Tierney R, et al. The Impact of Smad3 Loss of Function on TGF- β Signaling and Radiation-Induced Capsular Contracture. *Plastic and Reconstructive Surgery*. 2011;127(6):2263. doi:10.1097/PRS.0b013e3182131bea
 21. Brown KA, Pietenpol JA, Moses HL. A tale of two proteins: Differential roles and regulation of Smad2 and Smad3 in TGF- β signaling. *Journal of Cellular Biochemistry*. 2007;101(1):9-33. doi:10.1002/jcb.21255
 22. Hansen TC, Woeller CF, Lacy SH, Koltz PF, Langstein HN, Phipps RP. Thy1 (CD90) Expression Is Elevated in Radiation-Induced Periprosthetic Capsular

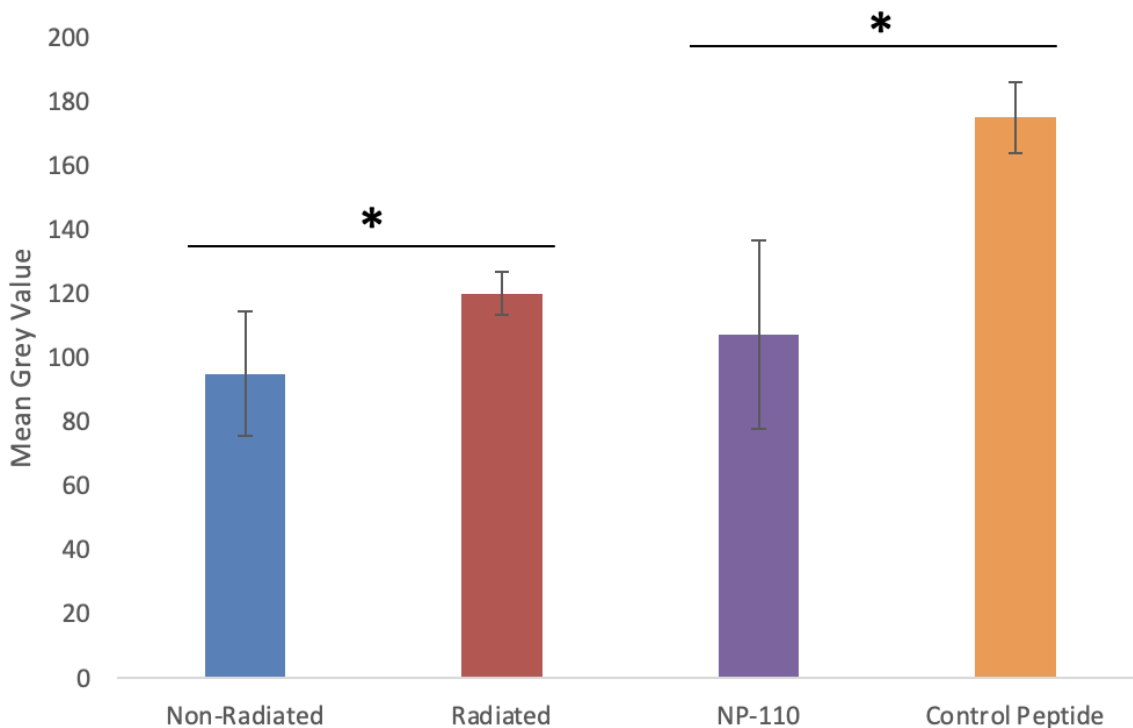
- Contracture: Implication for Novel Therapeutics. *Plast Reconstr Surg.* 2017;140(2):316-326. doi:10.1097/PRS.0000000000003542
23. Papaconstantinou A, Koletsa T, Demiri E, et al. Nonsurgical treatment of capsular contracture: Review of clinical studies. *J Int Med Res.* 2020;48(6):0300060520927873. doi:10.1177/0300060520927873
 24. Baker JL, Bartels RJ, Douglas WM. Closed compression technique for rupturing a contracted capsule around a breast implant. *Plast Reconstr Surg.* 1976;58(2):137-141. doi:10.1097/00006534-197608000-00002
 25. Lee HK, Jin US, Lee YH. Subpectoral and Precapsular Implant Repositioning Technique: Correction of Capsular Contracture and Implant Malposition. *Aesthetic Plast Surg.* 2011;35(6):1126-1132. doi:10.1007/s00266-011-9714-z
 26. Collis N, Sharpe DT. Recurrence of Subglandular Breast Implant Capsular Contracture: Anterior versus Total Capsulectomy. *Plastic and Reconstructive Surgery.* 2000;106(4):792.
 27. Chasan PE. Breast Capsulorrhaphy Revisited: A Simple Technique for Complex Problems. *Plastic and Reconstructive Surgery.* 2005;115(1):296. doi:10.1097/01.PRS.0000146706.85392.6F
 28. Rieger UM, Mesina J, Kalbermatten DF, et al. Bacterial biofilms and capsular contracture in patients with breast implants. *British Journal of Surgery.* 2013;100(6):768-774. doi:10.1002/bjs.9084
 29. Menkü Özdemir FD, Üstün GG, Kösemehmetoğlu K, İspirli M, Boynuydoğan E, Uzun H. Comparison of Cromolyn Sodium, Montelukast, and Zafirlukast Prophylaxis for Capsular Contracture. *Plastic and Reconstructive Surgery.* 2022;150(5):1005e. doi:10.1097/PRS.00000000000009653
 30. Woo SH, Kim WS, Bae TH, Kim MK, Park SW, Kim HK. Comparison of the Effects of Acellular Dermal Matrix and Montelukast on Radiation-Induced Peri-implant Capsular Formation in Rabbits. *Annals of Plastic Surgery.* 2020;85(3):299. doi:10.1097/SAP.0000000000002260
 31. Veras-Castillo ER, Cardenas-Camarena L, Lyra-Gonzalez I, et al. Controlled Clinical Trial With Pirfenidone in the Treatment of Breast Capsular Contracture: Association of TGF- β Polymorphisms. *Annals of Plastic Surgery.* 2013;70(1):16. doi:10.1097/SAP.0b013e31822284f4
 32. Garza RM, Paik KJ, Chung MT, et al. Studies in Fat Grafting: Part III. Fat grafting irradiated tissue: Improved skin quality and decreased fat graft retention. *Plast Reconstr Surg.* 2014;134(2):249-257. doi:10.1097/PRS.0000000000000326

33. Wang HC, Sun ET, Zhao RC, et al. Adipose-Derived Stem Cells Attenuate Skin Fibrosis and Improve Fat Retention of a Localized Scleroderma Mouse Model. *Plast Reconstr Surg*. 2023;151(1):97-107. doi:10.1097/PRS.00000000000009796
34. Bachour Y. Capsular Contracture in Breast Implant Surgery: Where Are We Now and Where Are We Going? *Aesth Plast Surg*. 2021;45(3):1328-1337. doi:10.1007/s00266-021-02141-6
35. Kim SE. Prepectoral breast reconstruction. *Yeungnam Univ J Med*. 2019;36(3):201-207. doi:10.12701/yujm.2019.00283
36. Larsen A, Rasmussen LE, Rasmussen LF, et al. Histological Analyses of Capsular Contracture and Associated Risk Factors: A Systematic Review. *Aesth Plast Surg*. 2021;45(6):2714-2728. doi:10.1007/s00266-021-02473-3
37. Kim HB, Han HH, Eom JS. Difference in the Occurrence of Capsular Contracture According to Tissue Characteristics in an Irradiated Rat Model. *Plast Reconstr Surg*. 2023;152(4):655e-661e. doi:10.1097/PRS.00000000000010387
38. Hauser-Kawaguchi A, Tolg C, Peart T, Milne M, Turley EA, Luyt LG. A truncated RHAMM protein for discovering novel therapeutic peptides. *Bioorg Med Chem*. 2018;26(18):5194-5203. doi:10.1016/j.bmc.2018.09.018
39. Cui Z, Liao J, Cheong N, et al. The Receptor for Hyaluronan-Mediated Motility (CD168) promotes inflammation and fibrosis after acute lung injury. *Matrix Biology*. 2019;78-79:255-271. doi:10.1016/j.matbio.2018.08.002
40. Wu J, Qu Y, Zhang YP, Deng JX, Yu QH. RHAMM induces progression of rheumatoid arthritis by enhancing the functions of fibroblast-like synoviocytes. *BMC Musculoskelet Disord*. 2018;19(1):455. doi:10.1186/s12891-018-2370-6
41. Hauser-Kawaguchi A, Luyt LG, Turley E. Design of peptide mimetics to block pro-inflammatory functions of HA fragments. *Matrix Biol*. 2019;78-79:346-356. doi:10.1016/j.matbio.2018.01.021
42. Tolg C, Messam BJA, McCarthy JB, Nelson AC, Turley EA. Hyaluronan Functions in Wound Repair That Are Captured to Fuel Breast Cancer Progression. *Biomolecules*. 2021;11(11):1551. doi:10.3390/biom11111551
43. D'Agostino A, Stellavato A, Corsuto L, et al. Is molecular size a discriminating factor in hyaluronan interaction with human cells? *Carbohydrate Polymers*. 2017;157:21-30. doi:10.1016/j.carbpol.2016.07.125
44. Cowman MK, Lee HG, Schwertfeger KL, McCarthy JB, Turley EA. The Content and Size of Hyaluronan in Biological Fluids and Tissues. *Front Immunol*. 2015;6:261. doi:10.3389/fimmu.2015.00261

45. Prantl L, Pöppl N, Horvat N, Heine N, Eisenmann-Klein M. Serologic and Histologic Findings in Patients with Capsular Contracture After Breast Augmentation with Smooth Silicone Gel Implants: Is Serum Hyaluronan a Potential Predictor? *Aesth Plast Surg*. 2005;29(6):510-518. doi:10.1007/s00266-005-5049-y
46. Tan KT, Baildam AD, Juma A, Milner CM, Day AJ, Bayat A. Hyaluronan, TSG 6 and inter α inhibitor in periprosthetic breast capsules: reduced levels of free hyaluronan and TSG 6 expression in contracted capsules. *Aesthet Surg J*. 2011;31(1):47-55. doi:10.1177/1090820X10391778
47. Tolg C, Hamilton SR, Zalinska E, et al. A RHAMM Mimetic Peptide Blocks Hyaluronan Signaling and Reduces Inflammation and Fibrogenesis in Excisional Skin Wounds. *The American Journal of Pathology*. 2012;181(4):1250-1270. doi:10.1016/j.ajpath.2012.06.036
48. Turley EA, Naor D. RHAMM and CD44 peptides-analytic tools and potential drugs. *Front Biosci (Landmark Ed)*. 2012;17(5):1775-1794. doi:10.2741/4018
49. Tolg C, McCarthy JB, Yazdani A, Turley EA. Hyaluronan and RHAMM in wound repair and the “cancerization” of stromal tissues. *Biomed Res Int*. 2014;2014:103923. doi:10.1155/2014/103923
50. Tolg C, Hamilton SR, Nakrieko KA, et al. Rhamm^{-/-} fibroblasts are defective in CD44-mediated ERK1,2 mitogenic signaling, leading to defective skin wound repair. *J Cell Biol*. 2006;175(6):1017-1028. doi:10.1083/jcb.200511027
51. Baker JL, Chandler ML, LeVier RR. Occurrence and activity of myofibroblasts in human capsular tissue surrounding mammary implants. *Plast Reconstr Surg*. 1981;68(6):905-912. doi:10.1097/00006534-198112000-00010
52. Dolores W, Christian R, Harald N, Hildegunde P, Georg W. Cellular and molecular composition of fibrous capsules formed around silicone breast implants with special focus on local immune reactions. *Journal of Autoimmunity*. 2004;23(1):81-91. doi:10.1016/j.jaut.2004.03.005
53. Wu KY, Kim S, Liu VM, et al. Function-Blocking RHAMM Peptides Attenuate Fibrosis and Promote Antifibrotic Adipokines in a Bleomycin-Induced Murine Model of Systemic Sclerosis. *J Invest Dermatol*. 2021;141(6):1482-1492.e4. doi:10.1016/j.jid.2019.11.032
54. Truong JL, Liu M, Tolg C, et al. Creating a Favorable Microenvironment for Fat Grafting in a Novel Model of Radiation-Induced Mammary Fat Pad Fibrosis. *Plastic and Reconstructive Surgery*. 2020;145(1):116. doi:10.1097/PRS.0000000000006344
55. Katznel EB, Koltz PF, Tierney R, et al. A Novel Animal Model for Studying Silicone Gel-Related Capsular Contracture. *Plastic and Reconstructive Surgery*. 2010;126(5):1483. doi:10.1097/PRS.0b013e3181ef8b8e

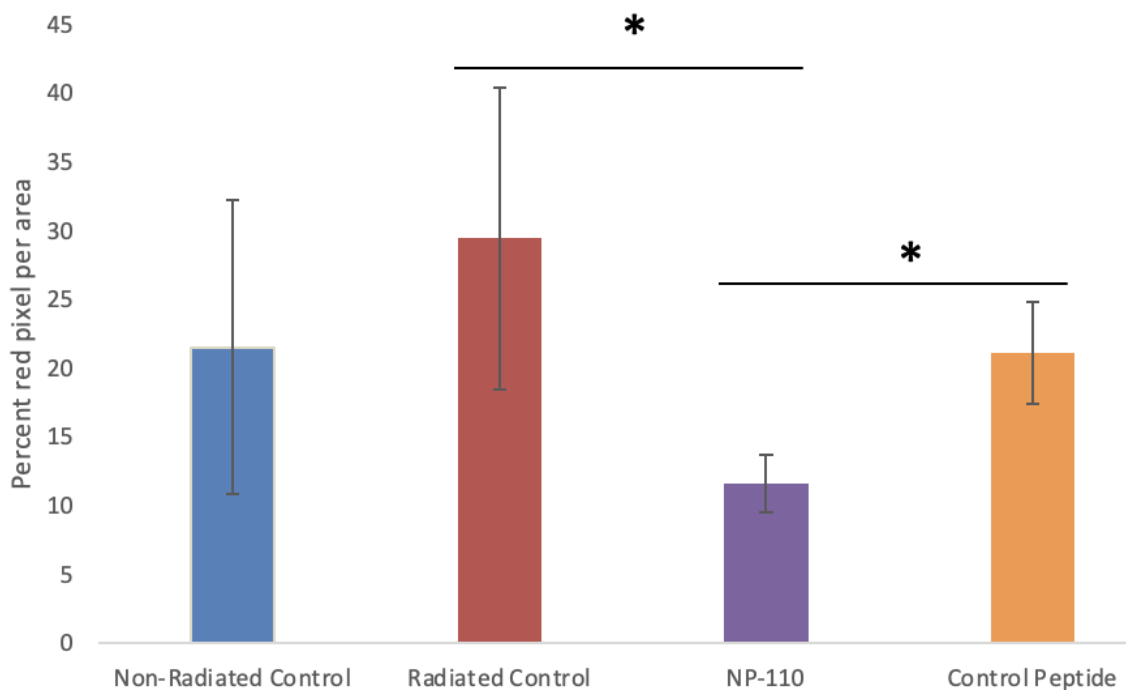
56. Kim JB, Jeon HJ, Lee JW, et al. A murine model of radiation-induced capsule-tissue reactions around smooth silicone implants. *Journal of Plastic Surgery and Hand Surgery*. 2018;52(4):217-224. doi:10.1080/2000656X.2018.1444617
57. Alexandra Lin, Sarah Karinja, Jaime Bernstein, et al. In Search of a Murine Model of Radiation-Induced Periprosthetic Capsular Fibrosis. *Annals of Plastic Surgery*. 2018;80(4):S204-S210.
58. DeLyzer T. *Development of a Novel Rodent Model of Radiation-Induced Implant Capsular Contracture*. Western University; 2022.
59. Charan J, Kantharia ND. How to calculate sample size in animal studies? *J Pharmacol Pharmacother*. 2013;4(4):303-306. doi:10.4103/0976-500X.119726
60. Kumar S, Kolozsvary A, Kohl R, Lu M, Brown S, Kim JH. Radiation-induced skin injury in the animal model of scleroderma: implications for post-radiotherapy fibrosis. *Radiat Oncol*. 2008;3:40. doi:10.1186/1748-717X-3-40
61. Sengupta P. The Laboratory Rat: Relating Its Age With Human's. *Int J Prev Med*. 2013;4(6):624-630.
62. Bell BI, Vercellino J, Brodin NP, et al. Orthovoltage X-rays exhibit increased efficacy compared to γ -rays in preclinical irradiation. *Cancer Res*. 2022;82(15):2678-2691. doi:10.1158/0008-5472.CAN-22-0656
63. Yarnold J, Brotons MCV. Pathogenetic mechanisms in radiation fibrosis. *Radiotherapy and Oncology*. 2010;97(1):149-161. doi:10.1016/j.radonc.2010.09.002
64. Weiskirchen R, Weiskirchen S, Tacke F. Organ and tissue fibrosis: Molecular signals, cellular mechanisms and translational implications. *Molecular Aspects of Medicine*. 2019;65:2-15. doi:10.1016/j.mam.2018.06.003
65. Leask A, Abraham DJ. TGF- β signaling and the fibrotic response. *The FASEB Journal*. 2004;18(7):816-827. doi:10.1096/fj.03-1273rev
66. Ehrhart EJ, Segarini P, Tsang MLS, Carroll AG, Barcellos-Hoff MH. Latent transforming growth factor β 1 activation in situ: quantitative and functional evidence after low-dose γ -irradiation. *The FASEB Journal*. 1997;11(12):991-1002. doi:10.1096/fasebj.11.12.9337152
67. Samuel SK, Hurta RA, Spearman MA, Wright JA, Turley EA, Greenberg AH. TGF- β 1 stimulation of cell locomotion utilizes the hyaluronan receptor RHAMM and hyaluronan. *J Cell Biol*. 1993;123(3):749-758. doi:10.1083/jcb.123.3.749
68. Hinz B, Celetta G, Tomasek JJ, Gabbiani G, Chaponnier C. Alpha-Smooth Muscle Actin Expression Upregulates Fibroblast Contractile Activity. *Mol Biol Cell*. 2001;12(9):2730-2741.

Appendix: Supplementary Materials



Appendix 1

Mean grey value of capsule samples, selecting for blue Masson's trichrome staining for collagen using ImageJ software. Higher mean grey value indicates increased darkness of stain uptake from the sample and therefore increased collagen. Data from the non-radiated and radiated group are shown from T. DeLyzer et al. for comparison to the NP-110 group and control peptide group. There was significantly increased collagen stain in the control peptide group compared to the NP-110 group ($p=0.004$). There was significantly increased collagen staining in the radiated compared to non-radiated control ($p<0.001$) from T.DeLyzer et al. data. When comparing the NP-110 to the non-radiated group there was no significant difference ($p=0.134$).



Appendix 2

Percent of red pixels per area of capsule samples, selecting for area of the capsules using ImageJ software. Higher percent red pixels indicates increased Picrosirius red stain from the sample and therefore increased collagen deposition and bundling. Data from the non-radiated and radiated group are shown from T. DeLlyzer et al. for comparison to the NP-110 group and control peptide group. There was significantly increased red staining in the control peptide group and the radiated control group compared to the NP-110 group ($p < 0.001$) when calculated with an independent two-tailed T-test.

Curriculum Vitae

Name: Kathryn Minkhorst

Post-secondary Education and Degrees: Queen's University
Kingston, Ontario, Canada
2014-2018 Bachelor of Science Honors (with Distinction)
Specialization in Life Sciences

Western University
Schulich School of Medicine and Dentistry
London, Ontario, Canada
2018-2022 Doctor of Medicine

Honours and Awards: McFarlane Research Award
Plastic and Reconstructive Surgery Department \$150
2024

Best Masters of Surgery Collqium Presentation Award
Masters of Surgery
2024

Lawson International Research Fund
Lawson Health Sciences, Research Grant \$15000
2023

Resident Research Grant
Schulich School of Medicine & Dentistry, Research Grant \$5000
2022

Dr. Fred N. Hagerman Memorial Prize in Surgery
Schulich School of Medicine & Dentistry, Graduation Award \$600
2022

Jimmy Sing and Sonia Mann Award in Pediatric Surgery
Schulich School of Medicine & Dentistry, Clerkship Award \$1500
2021

Summer Research Training Program
Schulich School of Medicine & Dentistry, Research Grant \$9000
2019-2020

Patient Centered Clinical Methods Course Award
Schulich School of Medicine & Dentistry
2019

Excellence in Research - Physiology
Queen's University, Graduation Award \$100
2018

Publications:

Wu KY, Kim S, Liu VM, Sabino A, **Minkhorst K**, Yazdani A, Turley EA. Function-blocking RHAMM peptides attenuate fibrosis and promote antifibrotic adipokines in a bleomycin-induced murine model of systemic sclerosis. *J Invest Dermatol.* 141(6):1482-1492, 2021.

AlGhanim K, **Minkhorst K**, Jaszkul K, Keelan S, Appleton S, DeLyzer T, and Yazdani A. Fat Grafting Versus Implants: Who's Happier? A Systematic Review and Meta-analysis. *Plastic Surgery.* 2023;0(0).

Jaszkul K., Farrokhi K, Castanov V, **Minkhorst K**, Li E, Sano L, Kim S, Keelan S, AlGhanim K, Simpson A. Global impact of lymphedema on quality of life and society. *Eur J Plast Surg.* 2023.

Minkhorst K, Castanov V, Li E, Farrokhi K, Jaszkul K, AlGhanim K, DeLyzer T, Simpson A. Alternatives to the DIEP flap in autologous breast reconstruction: A systematic review. *Annals of Plastic Surgery* 92(6):p 703-710, June 2024.

Presentations and Posters:

The use of NP-110, a RHAMM peptide mimetic, reduces capsule fibrosis in a novel rodent model of radiation induced capsular contracture

Minkhorst, K, Lewandoski, N, Turley, E, Wong, E, DeLyzer, T

Department of Surgery Research Day Masters of Surgery Keynote Presentation – June 5, 2024

Department of Plastic and Reconstructive Surgery Research Day – May 31, 2024

First Annual HMMR/RHAMM Symposium – October 17, 2023

The development of a rodent model for radiation induced breast capsular contracture

Minkhorst, K, Li, E, DeLyzer, T, Turley, E

Podium Presentation Canadian Society of Plastic Surgeons – June 16, 2022

Lawson Oncology Research and Education Day Poster Presentation – June 18, 2021

The profunda artery perforator and deep inferior epigastric perforator flaps for breast reconstruction: A systematic review

Minkhorst, K, Castanov, V, Li, E, Farrokhi, K, AlGhamin, K, Simpson, A.

American Society for Reconstructive Microsurgery Electronic Poster – January 15-18 2022

Association of Women Surgeons Regional Conference Oral Presentation – May 1, 2021

Thin-ALT and SCIP flaps versus standard ALT for lower extremity reconstruction: Is the evidence too thin?

Li, E, Farrokhi, K, Castanov, V, **Minkhorst, K**, AlGhamin, K, Simpson, A.

American Society for Reconstructive Microsurgery Electronic Poster – January 15-18 2022

London Health Research Day Electronic Poster – May 11, 2021